FAKULTÄT FÜR NATURWISSENSCHAFTEN

Otto-von-Guericke-Universität Magdeburg

Institut für Experimentelle Physik
Abteilung Nichtlineare Phänomene

Diplomarbeit

No more digging in the Dark

Investigating root growth in granular media with X-ray computed tomography

vorgelegt von
Caroline Bauer
geboren am 16.01.1990 in Magdeburg

verantwortlicher Betreuer
Prof. Dr. rer. nat. habil. Ralf Stannarius
Otto-von-Guericke-Universität Magdeburg,
Fakultät für Naturwissenschaften

inhaltliche Betreuung
Dr. rer. nat. habil. Matthias Schröter
Max-Planck-Institut für Dynamik und Selbstorganisation Göttingen,
Abteilung komplexer Fluide

Magdeburg, 5. Februar 2015

Contents

Präambel Hiermit versichere ich, diese Arbeit selbständig und ohne Benutzung anderer als der angegebenen Hilfsmittel angefertigt zu haben; die aus fremden Quellen direkt oder indirekt übernommenen Gedanken sind als solche kenntlich gemacht. Die Arbeit wurde bisher in gleicher oder ähnlicher Form keiner anderen Prüfungskommission vorgelegt und auch nicht veröffentlicht.

Acknowledgements

This thesis wouldn't have been possible without the help, encouragement, thoughts and spirit of many people:

Matthias Schröter, MPI-DS, for offering me a thesis supervision on a research idea that was enticingly crazy and funny and simple, at a place between the research fields where nobody had looked before and very Physics-like at the same time. – Well, it wasn't that simple, obviously, but the rest is still true. Also for all the meta discussions on physics and physicists, science in general, writing and presenting, meta-physics, society, love, kids, ... and for your encouragement and kind advices. It stands: Matthias:Caroline's inner devil = 2:0

Kai Huang, Experimentalphysik V at Uni Bayreuth: for the idea of this thesis and the help and ideas in the development of the growth cells.

Ralf Stannarius, OvGU: for the second external thesis supervision and probably quite some patience, and for the catalysis of quick bureaucracy help after the accident.

Ina Meier and Rebecca Liese, Albrecht-von-Haller-Institut für Pflanzenwissenschaften, Universität Göttingen: for the ideas and biology insight, and practical help with the nutrient solution and getting the project started.

Heinrich-Böll Foundation for the stipend supporting my physics education and providing a great environment for inspiring discussions and seminars on society.

Stephan Herminghaus, MPI-DS for hosting me at his department and thus providing me with the infrastructure necessary for this thesis.

Arnaud Hemmerle, André Schella, Meike Kunze, Simon Weis, Artur Wachtel: for the constructive feedback on the thesis and picking at all the details.

Markus Benderoth: for doing the job of "teaching you how to not kill yourself in the lab!" very well and adding his biology knowledge on top. Wolf Keiderling and the mechanics workshop here and at Bayreuth.

Corinna Maass, Quentin Brousseau, Stephan Herminghaus, Rainer Engelken, Deniz Pekin, Sibylle Nägle, Alexander Schmeink: for wonderful practical experience and meta discussions on social acoustics. Zrinka Gattin: for the green thumbed witch taking care of my office plants.Thomas Eggers: for being patient, friendly and helpful during computer problems. For becoming my first friend in Göttingen during all the DCF movie nights you and Antoine Fourrière organised and cooking and tea and talking and time.Simon Weis: for your detailed constructive feedback, sharing knowledge about X-ray tomography, packings (e.g. letting me use your program to calculate the pair-correlation function), and for being

a great office mate and friend during the last crazy weeks. Artur Wachtel, Martin Rohloff, Jürgen Vollmer: for a great time in Dresden, the dice of decision and an unexpected journey into the clouds.

All the other wonderful, kind people in the DCF family and those visiting me in hospital or making not walking easier and funnier. The poem is for you.

Benjamin Schäfer, Thomas Stöter: for the past 6 years of physics and everything. Let's see, what else life has in store.

Christine, Holger und Konstantin Bauer, Waltraudt und Jürgen Keuters, Angela Bauer: dafür, dass ihr mir die Familie seid, die ich mir wohl ausgesucht hätte, wenn wir uns nicht ohnehin erwischt hätten. Ich danke euch für eure geduldige moralische Unterstützung meiner Arbeit und meines Studiums, dass ihr auch dann mich glaubt, wenn ich es mal nicht tue und dass ihr euch Mühe gegeben habt, meine Erklärungen zu verstehen, wenn ich mal wieder Wissenschaftsjournalismus an euch geübt habe.

Cb

Wassermorgen

dcf

vor dem Tag
flieht
der Nebel
über den frühen See
tanzt
in Kreisen
den Traum
der eben vergangenen Nacht

– Edersee, 23.9.2014

To Earth.
May we never
cease
to be amazed by her
miracles. And to my
parents, machine and water engineers,
musicians and readers, keeping me on the
ground and rooted and
teaching me not to stop asking
questions.

1 Introduction

Harvest time. A vehicle the size of four elephants and three times as heavy rolls over the fields of Klein Wanzleben in the Magdeburger Boerde[1], collecting the sugar beets. The soil beneath its wheels is compacted by the roughly 25 tons into a depth of up to 90 cm. The consequences: the density of soil pores (*macropores*[2]) through which the roots are supplied with oxygen and through which water is transported to lower soil layers (*subsoil*) decreases, roots face a higher mechanical resistance (*impedance*) to their growth. The water and nutrient uptake decreases, the yield decreases, water erosion is advantaged: The soil degenerates.

This is already known (Lynch & Wojciechowski (2015), Zou *et al.* (2000), Chen *et al.* (2014)) and even made its way into the public press (most recently into the "Bodenatlas" (soil atlas) published by the German Heinrich-Böll Foundation, see for example the articles of Beste (2015) or (Ehlers, 2015)). Yet, it does not answer the following question:

> What exactly happens to the root on a bio-mechanical level as it encounters a denser soil layer? What happens physically to the soil, as it is traversed by the root during growth?

These questions are highly relevant to problems this human society is currently facing and, connecting physics and plant biology, they motivated me to start the present study. In this thesis I will present an experimental method that contributes to an answer to these questions.

However, before I delve deeper into my own approach, I shortly describe the already existing methods, their potentials and limitations.

1.1 Studying roots: state of the art

When scientists set out to study the root of a plant, they are faced with an obvious difficulty: usually roots grow in soil or sand or even break cracks into stones, all of which are intransparent materials. Classical methods developed so far are therefore either destructive to the root system, like washing away the soil for measuring root length or quantifying the root hierarchy (*root washing*, see e.g. the review by Neumann *et al.* (2009) or description in Heeraman *et al.* (1997)), or they circumvent the problem by exchanging soil with a transparent growth medium like water or gel (*hydroponics*, e.g.Hoagland & Arnon (1938) or Silverberg *et al.* (2012)). Root washing not only disallows an

[1] a fertile plain near Magdeburg, Saxony-Anhalt

[2] terms in *italics* can be found in the glossary on p.80

investigation of the temporal development of root growth, it also destroys finer root structures and *root hairs*, that play an important role in the interaction with the surrounding soil (*rhizosphere*, Meier *et al.* (2015)). Hydroponics and gel-based growth systems on the other hand neglect the physical interaction between the root and the soil (Hargreaves *et al.*, 2008). Following both conditions, intact roots *and* root-soil interaction, *root windows* (transparent panes lining previously dug holes in the ground adjacent to the studied plant, see Fig.1a) and *mini-rhizotron* tubes (hollow transparent cylinders protruding into the ground that are scanned from the inside with small cameras, see e.g. Neumann *et al.* (2009) or Withington *et al.* (2003)) pose the possibility to simultaneously study the imminent environment of a root visually. At the same time (bio-) chemical investigation of that precise region is facilitated, because soil samples are obtained directly from the region of interest with visual guidance from the root window. Root windows or rhizotrons may, however, introduce artefacts from water condensation, temperature gradients, different *soil strength* at the transparent pane or from chemical interaction between pane material and soil, as e.g. Withington *et al.* (2003) and Mooney *et al.* (2011) report. Furthermore, only 2D, not 3D information about root structure can be obtained.

More recently developed experimental techniques originate in physics, material science and/or medicine. Moradi *et al.* (2011) used neutron tomography (NT, see Fig.1b) to study the water content in the rhizosphere in 3D. The high sensitivity of the attenuation value of neutrons to the water content of a sample allows for a good separation between root and soil matrix.

Magnetic resonance tomography (MRT), as in medical studies, map fluid transport within the vascular system of a plant, both in roots and aboveground parts (Hillnhütter *et al.*, 2012), and provides structural information about the root (Poorter *et al.*, 2012). MRT is on the other hand hindered by ferro- and paramagnetic particles in soil which lead to poor signal-noise ratio (Moradi *et al.*, 2011).

The structure of the soil, i.e. its density distribution, cannot be obtained by either of them, though. This is where X-ray tomography comes into play.

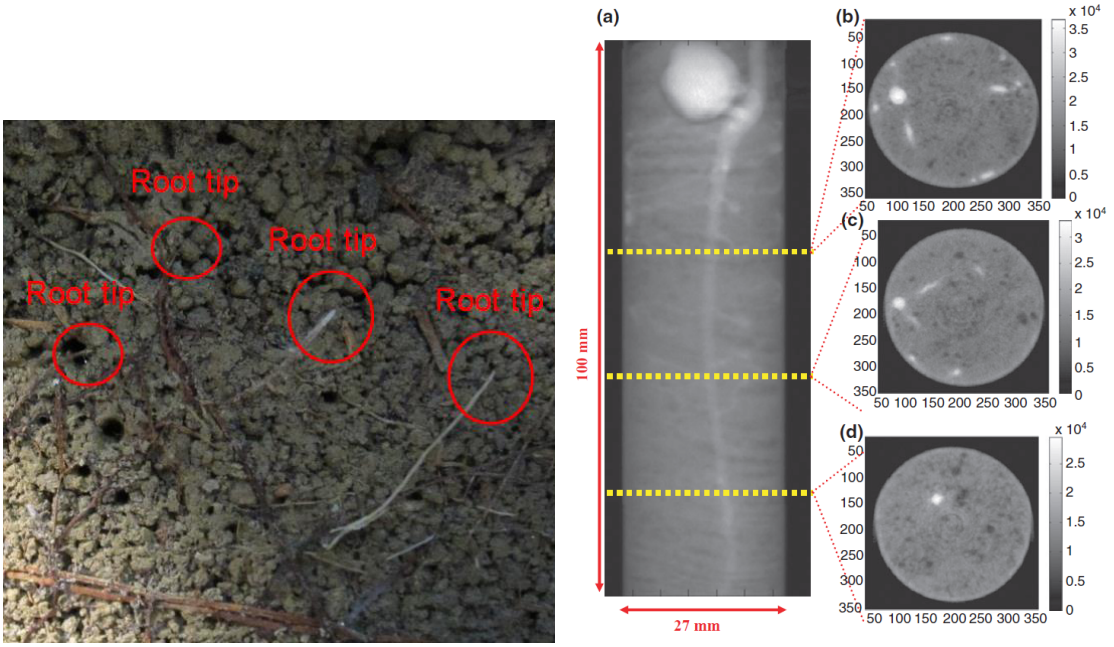

(a) root window (b) Neutron tomography

Figure 1: Root studying methods. LEFT SUBFIGURE: Image from a root window showing roots with root tips of a loblolly pine (taken from supplementals of Meier *et al.* (2015)). RIGHT SUBFIGURE: Raw data from neutron tomography of a twelve-day-old chickpea grown in sandy soil. Image (a) shows the tomogram from the side, (b)-(d) show horizontal cross-sections from the tomogram. The brighter the gray value, the higher the water content (taken from Moradi *et al.* (2011)).

1.1.1 X-ray computed tomography (X-ray CT) of roots

X-ray CT is a non-destructive method to study root architecture and soil structure in 3D based on the *attenuation* of X-rays (photon radiation) in materials. The attenuation depends mostly on atomic number of the chemical elements the material is made of, its density and width. The technique is 3D, because 2D X-ray images (*projections*) taken from all angles are reconstructed to yield a 3D image data set (*tomogram*).

In contrast to MRT it is not as heavily affected by magnetic soil particles and in contrast to both MRT and NT the soil structure, i.e. soil pores and density, is accessible with this technique. X-ray CT apparatuses are also more available than neutron sources needed for NT.

Using X-ray CT for the study of plants and plant roots started in the early 90's, coming from the direction of non-destructive soil analysis in plant and geosciences (Wantanabe *et al.*, 1992). It has been used so far to characterize

soil properties like *pore space*, bulk density, permeability for water or the water content in soil. The image parts that have to be separated in order to retrieve a 3D structure of the root are: root, solids (stone/sand particles), air-filled pores in the soil, water between solids, organic matter not belonging to the plant (e.g. bacteria or fungi). An example of this is provided in Fig.2b. Root properties obtained were, among others, length and diameter of roots, root development, water uptake, differences in root complexity between infected and healthy plants and root-induced soil compaction (as described in the review by Mooney *et al.* (2011) and references therein, e.g. Heeraman *et al.* (1997)). There have been few studies (Zappala *et al.*, 2013) on the interaction between roots and soil, though.

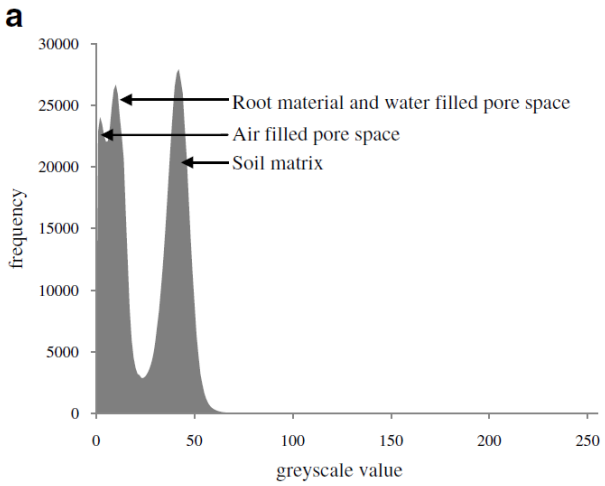

(a) Histogram

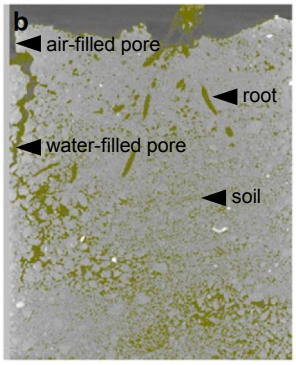

(b) Vertical cross-section of the 3D tomogram

Figure 2: A typical 50×60 mm soil sample (sandy loam) containing wheat roots visualized with X-ray CT. Note the similar attenuation values for roots and pore spaces. Greenish colour added after image processing highlights water and/or roots (original images taken from Mooney *et al.* (2011))

In most cases poor spatial resolution (voxel sizes similar to root diameter) and/or similar attenuation values between these parts prevent deeper investigation on root-soil interaction (as Fig.2 shows). They result from the inhomogeneity of the soil and the compromise between high X-ray intensity needed to penetrate silicium without damaging the plant(Zappala *et al.*, 2013). To overcome these difficulties sophisticated methods of image processing have been developed, ranging from global grey thresholds to local region growth that takes shape or colour or contours into account (Mooney *et al.*, 2011). This poses the questions:

Is it possible to reduce the complexity of the system root-water-soil in order to achieve a better image quality? Does a quantitative description based on root and soil parameters from these images yield a deeper insight into their mechanical interaction? For example: what makes a root force its way through compacted soil or, alternatively, when does it evade this region?

1.2 A physicist's reduction of the problem

Physicists like to reduce a problem to its essence. They create a theoretical or experimental model and assume, it applies to a wider set of problems with the same principal properties as the one they started with.

1.2.1 Soil as granular medium and/or root as penetrating rod

Silverberg *et al.* (2012) asked what happens to the root morphology when the stiffness of the medium the primary plant root penetrates is suddenly increasing at the root tip. They modelled the soil as a continuous medium: a transparent nutrient gel consisting of a pliable upper and a stiff lower layer. The imaging was done with a *laser sheet scan*. They observed that when the root tip hit the lower layer, the part above the tip buckled into a helix shape. Varying the stiffness of the lower layer they found that the root geometry and its variation depend strongly on that stiffness. Supported by a confocal microscopy analysis of the root structure, a mechanical model experiment with a metal rod and a theoretical model of the that rod they suggest this touch-activated twisting of the root to be an evolutionary mechanism of the plant to evade impenetrable barriers or force through rocks.

Wendell *et al.* (2011) decided to reduce soil to a two-dimensional granular medium of discs that have the same diameter and visualized the forces in that medium using a *stress-birefringent* (or *photoelastic*) material for the discs. They investigated how plant roots respond to the forces between grains and how the root changes these forces during growth. Their experimental apparatus consisted of a flat acrylic box standing upright and filled with stress-birefringent discs and mineral water, on top of which germinated pinto beans were placed, growing into the packing. A camera recorded the growth of the root and the stress development inside the discs. They found that the roots are not able to grow between grains subject to high forces, but that the maximum force they tolerate increases with their age.

A similar experiment was conducted by Kolb *et al.* (2012): In order to measure the radial forces exerted by a growing root on the surrounding medium and the roots morphological response to the restriction imposed by the medium, they devised a 2D setup also using stress-birefringent discs. Two discs formed a gap of distance δ between each other, simulating a soil pore. On top of the gap a germinated chick pea seed was placed in a wet foam with the root pointing downwards. Images of the growing root were taken and its diameter development measured as it grew through the gap. The force it exerted on the discs was inferred from the photoelastic response. They found, contrary to other studies (see review by Bengough & Mullins (1990)), that the root diameter before and after the gap did not correspond to δ, also the *root elongation* rate did not change whether or not the root was constrained by the gap. The result of the force measurement was that once the root was inside the gap the more narrow it was, the more force was build up by the root. Yet, the force build-up did not stop at a maximum force. Often, though, the root escaped the gap entrance by *circumnutation*, especially for small δ. This first experiment was followed by a microscopic analysis of the root samples. It showed that the outer cells of the root were compressed, but the *central cylinder* was not affected.

These experiments, however, are either conducted in two dimensions (Kolb *et al.* (2012),Wendell *et al.* (2011)), they also do not supply the plants with nutrients) or they use a continuous medium (Silverberg *et al.*, 2012), which does not resemble the granular nature of soil, because forces are distributed differently in continuous and granular media (Jaeger *et al.*, 1996). All of them also subject the plants to additional stress by permanently shining light on the roots due to their visualization methods.

1.3 My approach: X-ray CT of plant growing in sphere packing

In this thesis I aim to combine the advantages of X-ray CT as a technique fit to visualize root growth in three (or four, if time is counted) dimensions with the reductionist approach of using a *mono-disperse* granular medium instead of soil in order to study the mechanical interactions between a root and its environment.

1.3.1 Penetrating granular media

Matthias Schröter and collaborators (Schröter *et al.*, 2007) found in an experimental investigation that a granular packing of mono-disperse spheres

responses differently to a penetrating rod, depending on its *volume fraction* φ: They very precisely prepared glass sphere packings of different φ in the range of 57.1% to 63.3% ($\Delta\varphi = 0.1\%$) with water pumped in from below at certain flow rates. Then they slowly pushed in a flat-headed metal rod while measuring the penetration force.

The penetration force was always increasing with penetration depth (Fig.3), but the surprising fact was, that over a range of experiments with increasing φ the force at a certain depth not only increased (this would be intuitive: the denser the packing, the harder it is to push something into it), but that at $\varphi \approx 60\%$ the additional amount of force needed for the next higher volume fraction became much higher than below $\varphi \approx 60\%$. They call this dramatic change of the impedance of the granular medium a phase transition, which appears at the same φ for the filling hight change of the packing. The density where the transition arises appears to be affected by the frictional properties of the spheres, thus the critical φ may be different for non-spherical particles with edges.

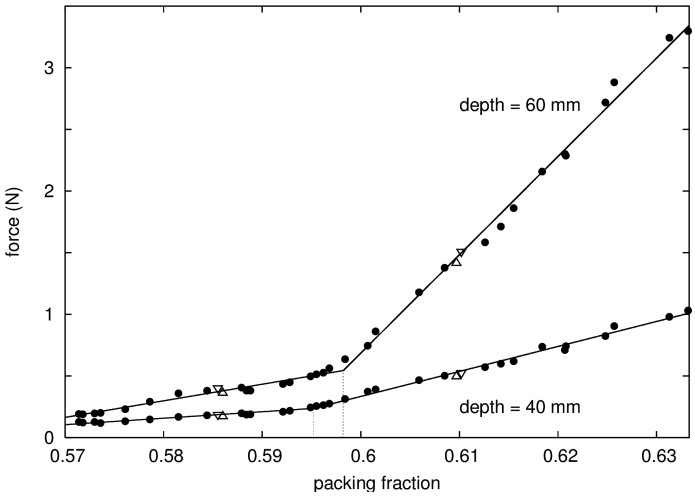

Figure 3: Force necessary to push a rod into a sphere packing as a function of its average volume fraction, measured at two penetration depths and speeds (different symbols). Image taken from Schröter *et al.* (2007)

However, if this generally true for granular media, i.e. that at a certain density it becomes suddenly increasingly difficult to penetrate the medium, this is also a situation a root faces during growth.

Therefore, I repeat the question already posed by Bengough & Mullins (1990) or Kolb *et al.* (2012) in the light of Schröter et al.'s finding:

Have plants evolutionary developed mechanisms to react to this

(as they call it) "phase transition" of the soil, i.e. does a root *know* that the impedance to its growth increases suddenly at a certain volume fraction?

Certainly, in view of findings presented by Chamovitz (2012) on the sensory system of a plant, the discussion of the topic by Cvrčková *et al.* (2009) or the discovery of the reaction of a plant's root to sound waves (Gagliano *et al.*, 2012), this appears not unlikely.

1.3.2 This thesis: developing a setup and code for tomogram processing

In this diploma thesis I present an experimental setup for investigating the root growth of Sinapis alba (white mustard) in a mono-disperse granular packing with X-ray computed tomography, as well as post-processing of the X-ray CT data with a self-written MATLAB routine.

Structure The structure of the thesis is as follows: First I provide background information on granular media, root growth and X-ray tomography in Section 2. Then I present a setup (Sec.3) fit to grow plants in a packing of dry mono-disperse spheres by supplying them with water and nutrients via an automated, closed fluid cycle, while monitoring humidity, temperature and illuminance. This is followed in Section 4 by a detailed description of the MATLAB code I developed for the detection of roots and sphere positions in 3D image data. In Section 5 I show the potential of the data generated with the setup and tomogram processing by measuring the volume of the root system with the acquired root position data and determining the sphere diameter by using a pair-correlation function of the sphere positions. At the end, in Section 6, in I draw a conclusion on the developed method.

How to use the thesis This thesis is supposed to be useful for the next person experimenting on plant roots in granular media and/or working with an X-ray computer tomograph. Since the topic has its roots in two rather disjunct scientific communities, plant biology and granular physics, often language and concepts used in one of them are not understood by the other. For this reason I will explain concepts or procedures in a way that hopefully a reader with either background is able to follow the text. At the end of the thesis (p.80) there is a glossary listing technical terms and jargon (written in *italics* at first appearance) to avoid misunderstandings like "hydro-culture" which for the average plant owner is a plant in clay granules but for the plant

biologist it is a plant grown completely in water. Details of experimental procedures or computer scripts are provided in the Appendix on page 77.

Names of software and manufacturers are written in SMALL CAPS, names of source code written by me or members of the group of Matthias Schröter is written in `typewriter style`.

A note for the next person working on this project: yes, please *do not hesitate* to ask any question about this work where the answer will make your work easier! If you ask me, I will send/give you the MATLAB code. I will even explain its documentation. My e-mail address[3] is

`caroline.bauer@posteo.de`

Note: similar research in other group As of October, 3 in 2014 it came to my knowledge via a short e-mail notice between my collaborator Ina Meier and Taryn Bauerle, that Bauerle's group is also doing X-ray CT on plants grown in a granular packing:

`https://sites.google.com/site/bauerlelab/research/root-competition`

However, this work has evolved independently from mine and so far I only know that their X-ray computer tomograph has similar specifications as the one I am using. Apart from that I have neither experimental details nor underlying scientific questions.

[3]Contact details will also be provided by Matthias Schröter. Encrypted e-mails are highly appreciated, by the way. This is the key ID: `0xDC72C152`.

2 Background

2.1 What are granular media?

Granular media consist of usually macroscopic particles ($> 1\,\mu$m) that interact via collisional, frictional contact with each other. On these length scales, quantum effects and random motion due to thermal energy (Brownian motion) are usually neglected. Examples for granular matter are sand, rocks, dust (depicting the span of length scales), grains, needles, marbles, pieces of ice (depicting classes of material and shapes), ...

Granular matter is categorized roughly into three phases: solid, fluid and gas. The names originate from the "ordinary" phases of continuous matter because of the many similarities they share. The categorization follows continuous matter by mainly using the density of the medium as the defining criterium, i.e. the ratio of particle volume and available space (*volume fraction, packing fraction*)[4]. In some aspects, however, due to its particular nature granular matter deviates from the behaviour of the phases we know. As a solid, the forces are arranged in a heterogeneous network, where some particles carry more load than others (Jaeger *et al.*, 1996). When granular matter starts to flow, meaning the particles move collectively, this force network is partly disrupted, but impetus and force is still transduced via the contacts (while energy of the system slowly dissipates because of the friction). This is why additional phase transitions as described by Schröter *et al.* (2007) can arise. Therefore, a homogeneous model (as the gel in Silverberg *et al.* (2012)) of soil will always be incomplete (Wendell *et al.*, 2011). It thus makes sense to use a granular medium as in the present study.

2.2 What is the principle of X-ray computed tomography?

X-ray computed tomography is a method to image the inner structure of an object in three dimensions.

Production of X-rays An X-ray source essentially consists of a current-heated (I_h) cathode that emits electrons, an anode (called *target*) that is hit by these electrons and a voltage source connecting anode and cathode and accelerating the electrons. Within the target two main effects appear that create X-rays (photons):

[4]Note, however, that granular matter is a field of very active research without a self-contained theory. Thus, definitions are bound to be "fuzzy".

1. The electrons hit atomic nuclei and are deflected by them – the energy lost during deflection is radiated in a broad wavelength spectrum of photons. The energy E of these photons depends on the trajectory and kinetic energy of the impacting electrons. The maximal energy is equal to the energy of the impacting electrons: $E_{max} = U_{acc} \cdot \mathrm{e}$.

2. The electrons hit electrons sitting in the inner atomic orbits. Those are removed from the orbit by the collision. The created gap is successively filled by electrons from a higher orbit which radiates photons with an energy characteristic for the difference between the orbits. Thus, these energies are discrete and depend on the target material.

Both effects add up to the resulting energy spectrum. Generally, a high acceleration voltage U_{acc} in the X-ray tube and a high number of accelerated electrons (which is determined by the heating current in the X-ray tube) leads to a high number of photons with high energies E.

Radiogram (2D projection) From the X-ray source the photons are directed towards the object that is to be imaged. In the object the photons are either absorbed (photoelectric effect, pair formation effect) or scattered (Rayleigh scattering, Compton scattering), which leads to an attenuation, i.e. a reduction of initial intensity I_0 of the X-ray beam. The law describing the attenuation is Lambert-Beer's law:

$$I(E) = I_0(E) \cdot \exp\left(-\int \mu(E,x)\mathrm{d}x\right) \tag{1}$$

with the absorption coefficient $\mu(E,x)$ depending on material density ρ, atomic number z, photonic energy E and object thickness x. The photons that pass the object have energies according to the matter they pass and are collected by a detector. It consists of a scintillating layer turning the high-energy photons into low-energy photons (visible light), which is recorded by a CCD camera. Thus, a projection of the object can be obtained.

3D tomograms from 2D projections With X-ray computed tomography a 3D image is produced by taking projections of the object from several angles (see Fig. 4), either with a rotating object (small objects) or a rotating source and detector (bigger objects, like humans) and computationally reconstructing them with an algorithm called filtered back-projection (for details, see Smith (1997)).

A tomogram is a three-dimensional image matrix of gray values that correspond to the attenuation of the beam at the respective points in the

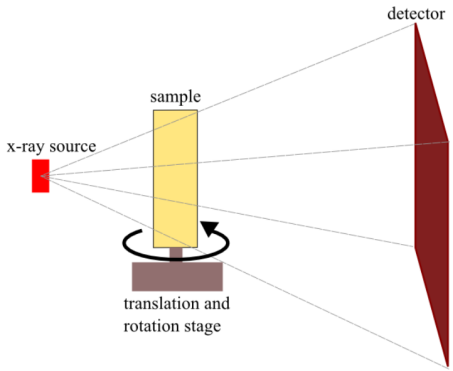

Figure 4: Principle of producing a X-ray computed tomography (taken from Murison (2014))

scanned object. Its smallest unit is the *voxel* whose edge length sets the lower limit of the resolution in the tomogram[5]. From the different attenuation values a 3D image can be obtained. The procedure I used for my experiments are described in Section 4 on p.43. In Fig. 5 an example for a projection, a cross-section of a tomogram and a 3D volume rendering are shown. A cross-section of the tomogram is called *slice*.

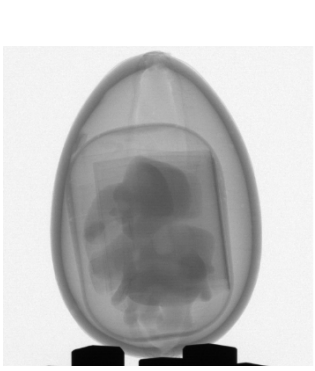

(a) X-ray projection

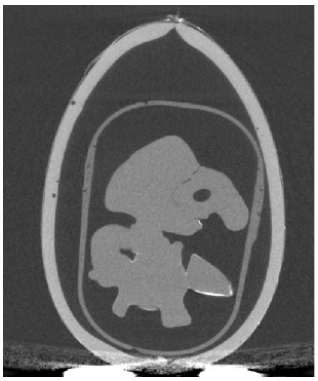

(b) Slice

(c) 3D volume rendering

Figure 5: X-ray CT stages of a kinder surprise egg: several projections are reconstructed to yield a tomogram consisting of several slices. The information therein can be used to create a 3D image with volume rendering. (Images taken from Murison (2014))

[5]Examples of artefacts reducing the resolution of the tomogram are provided by Platten (1998).

Considerations on X-ray parameters The effects leading to the attenuation of X-ray beams may ionize the molecules in the object they penetrate. Ionization by X-rays in living tissues can cause severe damages because of the uncontrolled destruction of molecules (proteins, DNA, lipids), disruption of chemical reactions in the cell cycle or the heat created during deceleration of electrons and photons. For medical applications, low energetic (15-60 keV) ("soft") X-rays are preferred to protect patient and physician, for material examination, "harder", more high-energetic X-rays (60-180 keV)[6] are used. On the one hand, the higher the energy, the stronger the signal that is collected by the detector. On the other hand, water has a low absorption coefficient compared to silicium or to plastic polymers and living matter consists to 80-90% of water (Strasburger *et al.*, 2008). My object of interest is a plant, therefore a rather low X-ray intensity both suffices to produce high-quality image and protects the plant from X-ray damage (more detailed considerations on this topic are provided in the following Section 2.3). This is also reflected in my choice of the material for the granular medium: a polymer with a low density and atomic numbers tremendously reduces the intensity needed for good image quality (in contrast to soil particles or glass spheres).

2.3 What effects do X-rays have on plants?

The quantity that measures the amount of X-rays taken up by organic tissue (plants, animals or humans) is the *dose D* with the unit Gy (Gray = Joule/kilogram). In essence, it is defined as the amount of energy per unit mass taken up by the tissue, but as the interdependency between tissue and X-rays are quite complex, it is hard to precisely determine how much energy is absorbed.

In a 10-year-study of 70 different plant species, Edna Johnson (Johnson, 1936) found that a moderate dose of 0.01-5 Gy[7] contributed to shoot and root elongation in young plants, if the dose was applied prior to germination and that plants subject to radiation after germination are more resilient. She notes that during early stages of growth, i.e. germination, plants are more affected by radiation, but in some cases (e.g. *Brassicaceae*) recovered as they reached maturity. In most cases the dose that significantly reduced plant growth was greater than 33 Gy, but the reaction to radiation varied across the investigated species, with affected growth at a dose as low as 0.05 Gy.

In another study by Zappala *et al.* (2013) the effect of X-rays on rice root growth was investigated. Using the same X-ray computer tomograph as in this

[6] or higher, depending of the capability of the apparatus

[7] An actual dose of more than 4 Gy is considered lethal to humans(Zappala *et al.*, 2013).

study and higher X-ray parameters they find at a dose of 13 Gy per plant no significant changes to root growth. The question of this section can therefore not be conclusively answered for "plants in general", so that statistically meaningful control experiments must be conducted species-wise. For a single species this requires three sets of plants grown in the same environmental conditions. Of these one is subjected to repeated radiation, one subjected to the conditions in the X-ray lab without scanning and the third not taken out of the growth environment at all. This is not within the scope of the present study.

2.4 What are mikorrhiza?

Mykorrhiza are a class of fungi that interact symbiotically with the plant roots. They are categorized by the root part they inhabit: either attached to the root on the outside (ektomykorrhiza) or partly (arbuscular mykorrhiza) or completely (endomykorrhiza) living in the inner or outer layers of root cells. The symbiosis partners of the most common form, the arbuscular mykorrhiza, are flowering plants (*angiosperms*). They form vesicles or tree-like structures in the outer cells of the root. The fungus replaces root hairs and supplies the plant with nutrients, while the plant supplies the fungus with carbohydrates. This more efficient nutrient supply, despite the release of sugars to the fungus, leads to a better plant growth. Plants with mykorrhiza also tend to be less susceptible to pathogenic fungi or *nematodes*. The biochemical interaction between a plant and its fungus is still an open question. (Abridged and translated from Strasburger *et al.* (2008).)

As the present study intends to reduce the interaction between root and soil to its mechanic component, a poorly-understood symbiosis is not welcome.

3 Setup and Experiment

Usually plants are not grown in a granular aggregate of plastic particles, not even in plant science. In this section I describe the necessary adjustments I apply to make them grow nonetheless. I start with the requirements that influence the decisions on plant type, granular particles and the shape of the growth cell. The constraints are met by the design of the growth cell and a tailor-made automated water supply system. Their descriptions are followed by the recipe of the nutrient solution and the measurements of the conditions under which the individual plants grow. A typical experiment from germination to the X-ray computed tomography (CT) scans is described at the end of the section.

I carried out the experiments at the Max-Planck-Institute for Dynamics and Self-Organization, with exception of the growth experiments described on p.23. These took place at the root lab of the Albrecht-von-Haller Institute for plant sciences of the Göttingen University with support of Ina Meier and Rebecca Liese. As the transport between root lab and X-ray lab could not be organised in a way not disturbing the plants and the granular packing, the controlled climate chambers of the root lab could not be used for the X-ray experiments.

For biological terms see the glossary on p.80, for longer explanation see section 2.4 on p.20. The principles of X-ray computed tomography are explained in section 2.2 on p.16.

3.1 Decision making: plants and particles

3.1.1 Plant: requirements and decision

1. **Relevance**
   The plant species should either be well-studied (e.g. known genom) or a biological model organism for a larger class of scientific questions or industrially relevant.

2. **Complexity**
   To maintain the simplicity of the system, the plant should not be in symbiosis with mykorrhiza (root fungi) or rhizobia (root bacteria), because the symbiotic interactions of roots with other organisms are still poorly understood (see Section 2.4 on p.20 for explanation).

3. **Time scale**
   Root growth should be fast enough so that several plants can be grown

in a few weeks by a single person, but not faster than 1 cm per day so that there are no movement artefacts on the CT scans.

4. **Adaptability**
   The plant should survive short (30-90 min) periods of complete dryness as well as several degrees (5-10°C) of temperature change, so that it can be taken to the Xray tomograph and back without additional water supply.

5. **Root thickness**
   The roots of the plant should have a diameter that is comparable to that of the particles, so that the root has to push its way through the packing like it does with soil (in contrast to large stone rocks). The root should also be thick enough to be well resolved by the computer tomograph.

6. **Scalability**
   Plant size, growth rate and the setup necessary to provide it with optimal growth conditions should allow for an increase the number of parallel running experiments.

White mustard, or *Sinapis alba L.* (Fig.6) is a *dicotyledon* from the family of *Brassicaceae*[8]. It is naturally growing in the mediterranean climate zone on calcareous soils(Clapham *et al.*, 1962). As one of only few plants it neither lives in symbiosis with a root fungus (*mykorrhiza*), nor does it develop root nodules in symbiosis with bacteria (*rhizobia*) for nutrient storage. This was one of the main reasons for this decision.

The genom of white mustard is not yet sequenced, however, it belongs to the same family as the genom-sequenced biological model plant *Arabidopsis thaliana* (Strasburger *et al.*, 2008) and it is used as a model plant itself in root growth studies (e.g.Lohmann *et al.* (2009),Fargašová (1999)). White mustard is industrially relevant due to its usage as a forage crop and as the main ingredient of mustard (see for instance Tabtabaei & Diosady (2013)). Its uses as a medical plant are documented back to the Antique (Mayer *et al.*, 2002).

The annual plant reaches a height up to 1.2 m, so that it is growing 1,20 m/6 months $\approx$ 7 mm/day. Expecting a comparable root growth, a root system of 4-6 cm length will have developed within 7-10 days, which fits the size limitations of our X-ray tomograph (13 cm from center of the beam to

[8]L. is the author's abbreviation for the botanical naming convention, in this case Carl Linneaus

ceiling of the tomograph). At that size the main root has a diameter of about 0.5 mm at the tip and 2 mm where it turns into the stem of the plant.

Figure 6: Botanic sketch of white mustard showing the above-ground parts of the plant. The name comes from the colour of the seeds, however, due to the colour of the flowers it is also referred to as yellow mustard (image from Brandt *et al.* (1883))

Estimating the growth rate of yellow mustard in granular media: The growth rate found in the literature assumes soil as the growth medium. It was therefore necessary to test whether this growth rate is comparable to that in a granular medium. For measuring an approximate growth rate I carried out growth tests with white mustard in a fully temperature and humidity controlled greenhouse in the root lab at the Göttingen University (see photo in Fig.7 on p.24). They showed that the mustard plants grew approximately

5 mm per day in polypropylene spheres (see p.24) under conditions of 60% relative humidity and 24°C (day)/18°C (night). The nutrient solution was delivered per hand every 48 hours in portions of 10 ml (recipe see Appendix p.79).

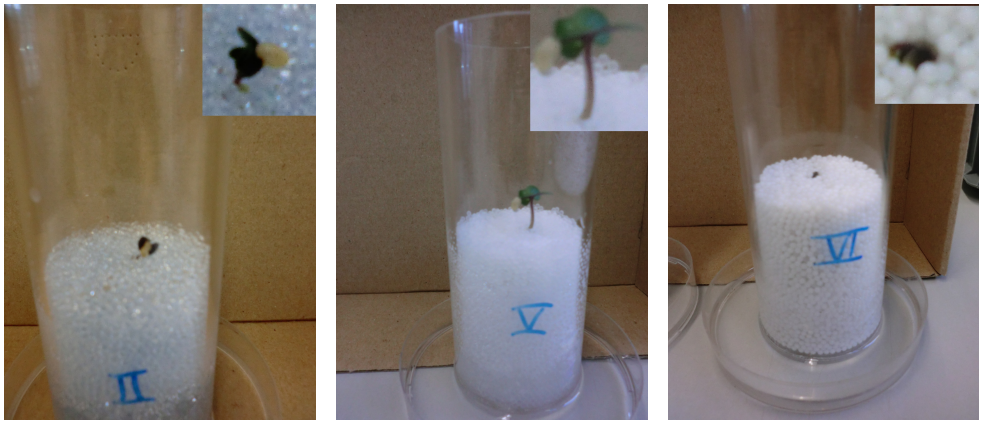

(a) glass
$d = 2$ mm
inset view from above

(b) polypropylene
$d = 1.85$ mm
inset side view

(c) polyoxymethylene
$d = 2$ mm
inset view from above

Figure 7: Root lab growth tests: White mustard, 5 days old, growing in packings of different sphere materials (a-c). The diameter of the growth cells is 4 cm. The yellowish object adhering to the leaves is the seed hull.

3.1.2 Particles: requirements and decision

- **Shape**
  As this is a reductionist approach to the system, image processing (particle finding) and the analysis of the packing should be as simple as possible. Therefore, I use monodisperse spherical particles.

- **Size**
  The sphere diameter should be smaller than 2 mm in order to comply with the German definition of *fine earth* (Strasburger *et al.*, 2008).

- **Price** The lower limit of the size was set by the price. Example: two growth cell fillings (60% packing fraction) cost 680€using 25,000 POM spheres of 2 mm vs. 1620€for 60,000 POM spheres of 1.5 mm from the same manufacturer.

- **Material**

  - It should be bio-chemically inert, so that the interaction of plant and particles is purely mechanical.
  - The material and the water should have a good contrast on the X-ray tomograms.
  - The X-ray intensity necessary to get a good image quality should neither damage the plant due to the Xray, nor should it be necessary to set the scan time to more than 90 min for the whole cell. After all, during that time the plant will be without water.

- **Quality**

  - Dispersity: The diameter of the particles should have a maximum dispersity of $d \pm 5\%$ for the calculation of the packing fraction.
  - Defects: The amount and size of defects within the particles should be minimal for easier image processing.

To test the contrast and defectiveness of the materials, I ordered a sample of two materials, grew a plant their respective particle aggregates and took computer tomograms. The images in Fig.8 are raw data example slices (2D image from the 3D tomogram) of both tomograms.

Fig. 8a shows that the POM spheres have many defects insde and that the root will be difficult to segment from the particles. Fig. 8b on the other hand shows a better contrast between sphere material and water/roots and close to zero defects. Therefore, I decided on the **Polypropylene** spheres.

Another reason leading to this decision was a good storage of nutrient solution within the packing, which I observed during the growth tests: the POM packing did not keep the fluid, so the plants dried out, whereas the PP packing hold it very well. Unfortunately, this later turned out to be a problem during image processing, because the root could not be separated from the water, if they were in direct contact. How I dealt with this problem is described in Sec.3.3.5 on page 33.

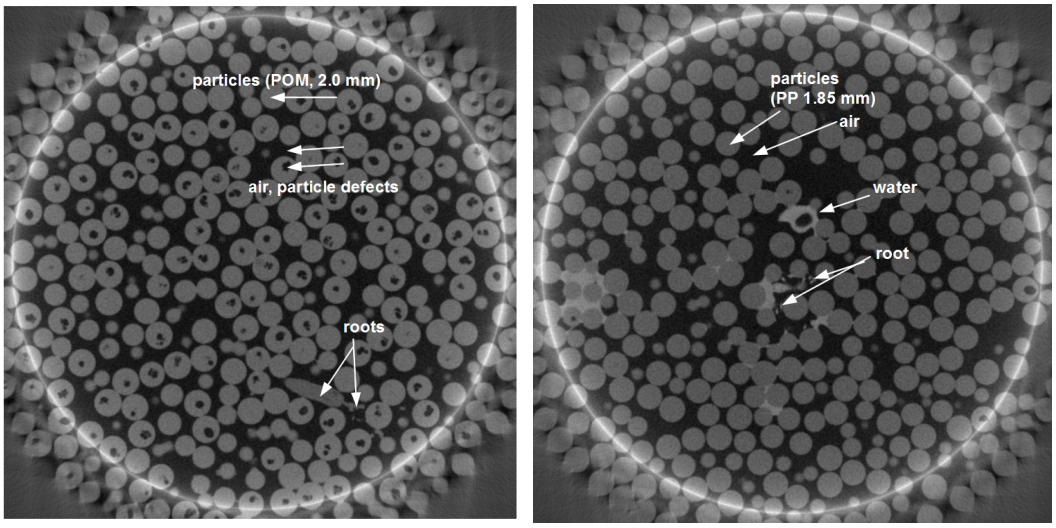

(a) Polyoxymethylene (POM)
$d = 2.00\,\text{mm}\ \pm 0.025\,\text{mm}$ (1.25%)

(b) Polypropylene (PP)
$d = 1.85\,\text{mm}\ \pm 0.03\,\text{mm}$ (1.6%)

Figure 8: Comparison of image contrast and particle quality for two particle materials using raw *slices*. These are 2D cuts through 3D tomograms perpendicular to the rotational axis of the cylindrical growth cell ($d = 4.4\,\text{cm}$). The white ring is a CT artifact.

3.2 Growth cell design

The design of the growth cell, especially in combination with the water supply, experienced several development stages. Here the final stage is described. A schematic of the assembled cell including the placement of the sensors and water supply is provided in Fig.9 and a photo of the assembled cell is shown in Fig.10. The technical drawing of the growth cell made by the Bayreuth mechnics workshop where the growth cell was built can be found in the Appendix (p.77).

The growth cell consists of two separable plexiglas cylinders: The top one ($l = 10\,\text{cm}$,$d_{\text{inner}} = 5\,\text{cm}$) can be taken off for transport and CT scans, it carries the water supply and sensors for monitoring temperature, relative humidity and illuminance while protecting the plants from draught. The bottom one ($l = 12\,\text{cm}$,$d_{\text{inner}} = 4.4\,\text{cm}$) is filled with the PP spheres,that serve as growth medium for the mustard plants. The sphere packing rests on a plastic plate with holes ($d = 5\,\text{mm}$) acting as a drainage for the nutrient solution. The plastic plate itself is covered by a gauze so that the spheres are not falling through the holes. A funnel leads the nutrient solution into a tube to the outside of the cell. The flow back into the storage container

is controlled by a manual valve. This valve also prevents leackage during tomography scans.

The growth cells were positioned on a lab windowsill of a window pointing South-East (Fig.10). I covered parts of the window with sheets of white paper to decrease the amount of direct sunlight, which heats up the air inside the cell. I also wrapped the cell in two layers of black and white paper to shield the roots against sun light and to keep the packing from heating up.

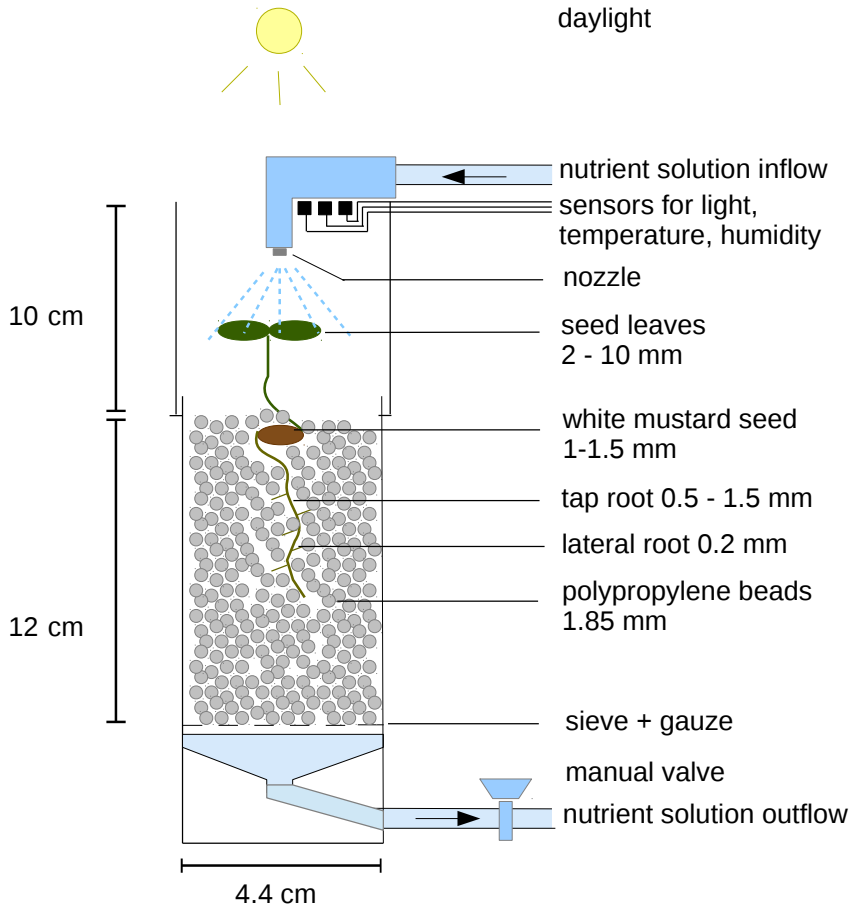

Figure 9: Schematic of growth cell with spheres and plant inside. Numbers refer to diameters unless noted otherwise.

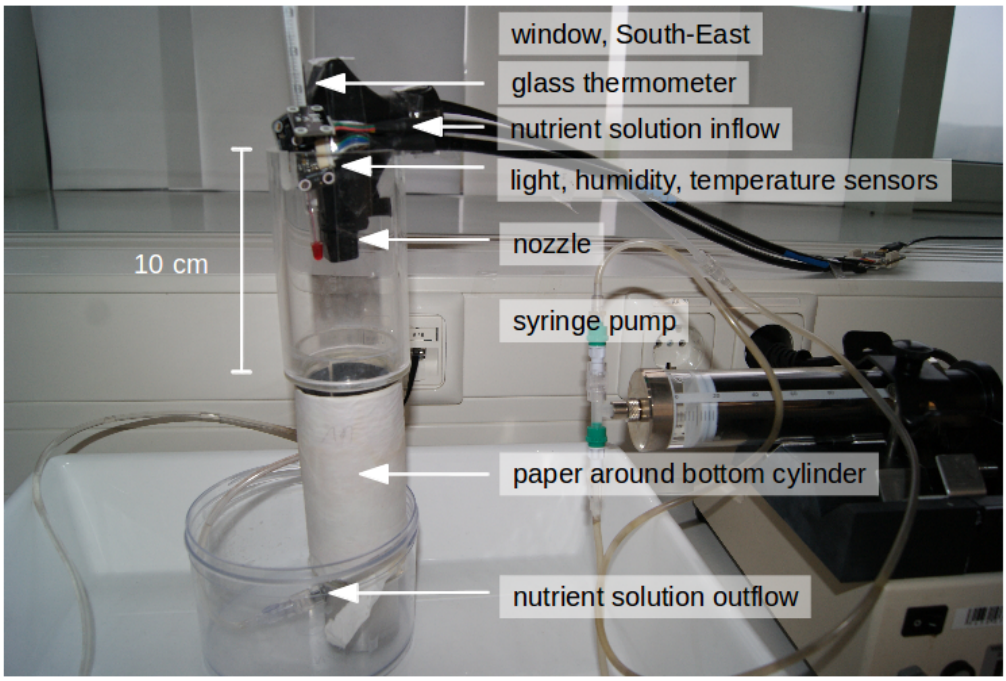

Figure 10: Photo of one assembled growth cell: the sensors, a liquid-in-glass thermometer and the nozzle were taped to the top cylinder, which could be taken off. The bottom cylinder is wrapped with paper as a protection. White paper sheets taped against the window pane act as a sunshade.

3.3 Water and nutrient supply

The most difficult part of the setup was to provide the plants with water and nutrients. The supply system had to comply with a range of conflicting criteria that are described in the following Section 3.3.1. The final stage of the system is described in Sec. 3.3.2 (p.29). Approaches that did not work are addressed in Sec.3.3.3(p.32). The composition of the nutrient solution (NS) is described in Section 3.3.4 on page 33 and in the Appendix.

3.3.1 Requirements

1. the amount necessary for the plants to grow:
    - The roots should never be completely dry, otherwise the plant starves because it cannot take up nutrients and water
    - The roots need to have access to oxygen. Flooding the growth cell is not an option because pumping oxygen in from below would

disturb the granular packing

- Especially in its first growth phase the plant looses a high amount of water by evaporation at the leaves, because they do not have developed a wax layer yet. Therefore, the fluid supply has to maintain a high humidity level in the air surrounding the plant.

2. The supply system should be automatic, so that the plants do not fall dry on weekends/during the night.

3. The fluid should neither mechanically disturb seedling nor packing.

4. The fluid should also not stay within the packing, because in the tomograms the water cannot be segmented from the root during image processing, if they in contact.

5. The supply system should create a homogeneous nutrient distribution to avoid that the root is following the nutrient/water gradient.

6. The population of microorganisms like algae should be kept low to prevent clogging of the tubing system.

3.3.2 Automated closed-cycle system

Cycle: Figs.11 and 12 show the final version of the system used to transport the NS from the reservoir to the growth cell and back: A LabVIEW-controlled syringe pump draws NS from the reservoir into a syringe and pumps it into the growth cells. From there the fluid is pumped to the reservoir again with a peristaltic pump. The tubes used for this are extension lines (type "Heidelberger"[9]) of 5 mm diameter, in which the flow is regulated by tees and non-return valves. The infusion parameters for the syringe pump are provided in Table 1, the technial details on p.30. The peristaltic pump is described on p.30. With this system two growth cells can be supplied with NS at the same time. The restricting factor is the syringe pump, which holds only two syringes at the time.

NS distribution at growth cells The method for infusing NS into the growth cells that fullfilled the criteria in Sec. 3.3.1 on p.28 best was connecting the nozzle of a spray bottle to the extension line leading to the syringe pump and place it at the top of the growth cell (see Fig.10 for close-up), pointing downwards. I tried different nozzles and decided on the one with least dripping at low NS pressure (no mechanical disturbance of packing!), finest

[9] they are usually used for blood/medicine infusions in hospitals

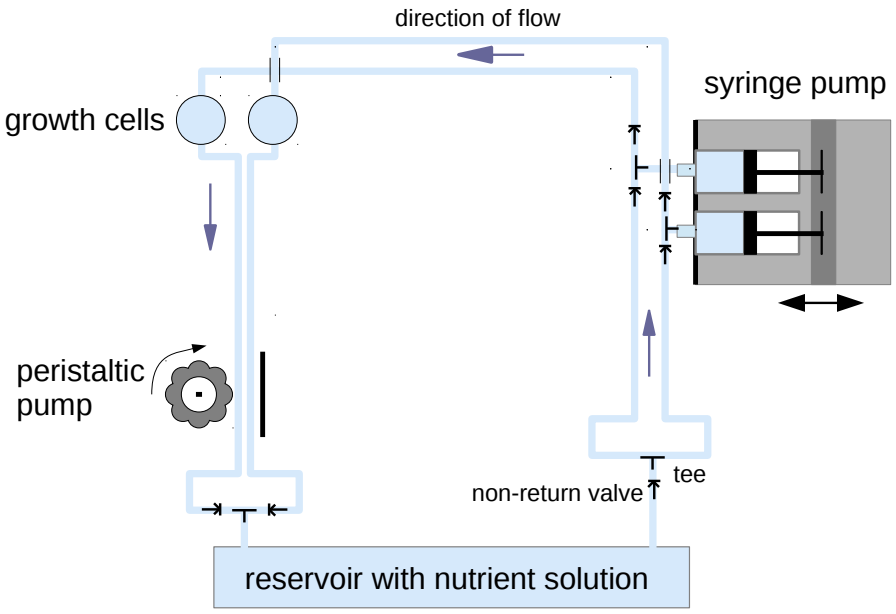

Figure 11: Sketch of the final automatic water supply and drainage system. The syringe pump was set to infuse 5 ml into the growth cells every 30 minutes, the peristaltic pump removed it every 60 minutes.

spray (homogeneous fluid distribution across the growth cell cross-section) and the least minimum flow rate necessary to produce a spray.[10] The limit to the flow rate was set by the syringe pump in combination with the syringe diameter.

Syringe pump: Harvard Apparatus, Syringe infusion pump 22 I/W A-27501.
Precision of infused volume at given parameters: 1 ml
Controlling: LabVIEW code written by Matthias Schröter with slight adaptions (`Cb_manage pump with polling.vi`) The infusion parameters are provided in Tab.1. They were found after several iterations of plant growth (see Sec.3.5.4 for details).

[10]It was a no-name product from a local garden center.

Table 1: Infusion parameters for the NS

syringe diameter:	35 mm
flow rate:	45 ml/min
infused volume:	5 ml every 30 min

Removing water from growth cells: Peristaltic pump ISMATEC, Reglo Pumpe Digital 4/8 ISI4834C.
Gravity driven drainage via an extension line to the reservoir 1 m below the growth cells was not enough to prevent flooding of the growth cells. The pump is connected to the extension line and draws NS from the cells every 60 minutes for 15 minutes.

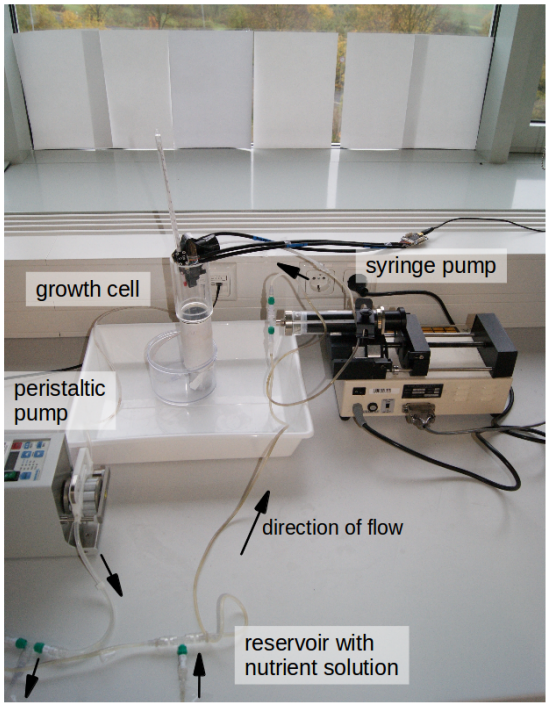

Figure 12: Photo of nutrient solution supply and drainage system: the placement of the parts corresponds to Fig.11, except for the reservoir, which is placed below the table. Black arrows indicate direction of flow. For clarity only one growth cell and accompanying tube system is shown.

3.3.3 Approaches that did not work

Fluid supply I: dripping from above The first idea was to let the NS drip into the growth cell from above (see Fig.13). This was hard to control. The drops repeatedly disturbed the packing and washed away the plant.

Figure 13: Fluid supply I: water dropping from end of Heidelberger Verlängerung washed away the plant and disturbed the packing.

Fluid supply II: glass ring The second approach was to use a glass ring (see Fig.14, designed and manufactured at Uni Bayreuth) that had 6 1.5 mm-sized holes on the bottom side. Water would then drip from the holes from a low height onto the plant and the sphere packing. However, the minimum flow to maintain a homogeneous dripping from all holes was too high, such that the packing was disturbed. If the flow rate was smaller, the plant would sometimes not receive any water at all and dry out.

lid on growth cell: humidity increase? An earlier version of the growth cell assembly contained a lid to be placed on top. This was supposed to create a closed greenhouse, where the water cannot evaporate and the humidity is kept high to protect the young plant from water loss. However, this caused the air inside to heat up well above 30°C, so I removed it.

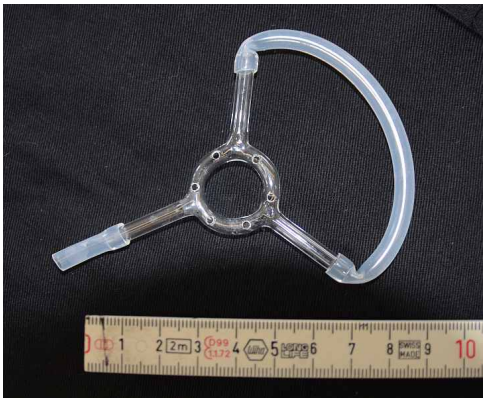

(a) Glass ring

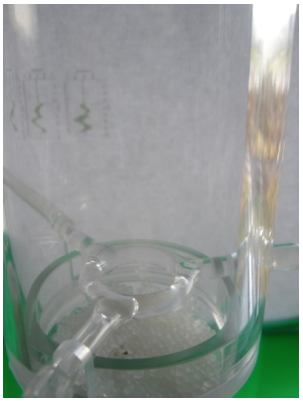

(b) Glass ring in setup

Figure 14: Glass ring: the water supposed to drop from small holes in low height onto the granular medium did not distribute the water homogeneously

3.3.4 Nutrients

One method to study root growth is growing the plant in water with oxygen pumped in from below. Since the water is the only nutrient source, it has to be enriched with all the nutrients the plant needs. This situation is quite similar to my situation, where the plant sits in a substrate (the PP spheres) that cannot supply it with nutrients. The nutrients used depend on the composition of the plant tissue, not on the soil composition. `insert ref to webpage soils.wisc.edu...` Therefore, the recipes for nutrient solutions are quite similar to each other and the most commonly used is a variation of Hoagland's solution (Hoagland & Arnon, 1938). A reference for the modified version I use is in Epstein & Bloom (2004)) and in Tab. 7 in the Appendix.

3.3.5 Surfactant within nutrient solution

The NS sprayed onto the granular aggregate sinks in only very slowly. This can result in a large droplet sitting on top of the aggregate, drowning the seedling. To deal with this problem, I add a surfactant (Tween20, mixing ratio with NS 1:800) to the NS. It reduces the surface tension of water and enhances the percolation into and through the granulate.

The addition of surfactant also solves a second issue: The living root contains roughly 85-90% water (Strasburger *et al.*, 2008). Therefore, it is not distinguishable from water droplets adhering to it on the CT slices. Having a decreased surface tension, the NS forms less droplets inside the granulate, thus facilitating more accurate detection of the roots.

Does the surfactant influence the development of the seedlings? To answer this question I conducted the following control experiment (see Fig.15): After germination 10 seeds were placed on moist cotton wool, of which one half was watered with NS containing the surfactant, the other half received normal NS. After 16 days I cut the plants off just above the cotton wool and dried them at 50 °C in a drying oven for 24 h. The resulting dry masses are provided in Tab.2. The standard deviation of the dry mass of treated plants, i.e., their growth variability, is wider than that of untreated plants, which means the plants do react differently when their NS contains a surfactant. However, the difference of the mean dry masses is so small that their standard deviations overlap.

Therefore, I conclude that for the 13 plants grown with treated NS during the X-ray experiments (Tab.5) the surfactant has no significant effect on their growth.

(a) with surfactant (1:800) (b) without surfactant

Figure 15: White mustard grown on cotton wool (day 4), one sample received nutrient solution with, the other without surfactant TWEEN20

Table 2: Dry masses of above-ground parts of 16-day-old mustard plants grown on cotton wool. One sample received Hoagland's modified nutrient solution (Epstein & Bloom, 2004) treated with surfactant, the other received untreated NS. All masses in mg ±0.7 mg.

	untreated NS	treated NS
	20.2	38.6
	52.9	55.3
	44.3	50.7
	23.2	39.6
	21.2	59.0
mean dry mass	32.4	48.6
standard deviation	13.6	8.2

3.4 Growth conditions: light, temperature and humidity

I grew plants and scanned them in the X-ray tomograph at the end of February (plant 1-4) and from the end of April to the end of June (plant 5-19). While the plants grew inside on the windowsill of a lab, the sunlight coming in from the South-East window is coupled to the season of the year and fluctuating weather conditions. Therefore, I measured illuminance, temperature and humidity within the growth cell.

For monitoring these conditions I used the humidity, temperature and ambient light bricklets from TINKERFORGE, which were controlled via a master brick. A shell script combining the respective C-programs of the bricklets collected the data and stored it in a file. The script is provided in the Appendix on p.78. The placement of the sensors is shown in Figs.9 (p.27) and 10 (p.28). Precision and range is provided in Tab.3.

Table 3: Name, Range and precision for sensors within Tinkerforge bricklets.

Ambient light	TEMT600, Vishay
illuminance range:	[0,900] lux
resolution:	0.1 lux
angle of half sensitivity:	60°
wavelength of max. sensitivity:	570 nm
operating temperature:	[-40,85] °C
tech. datasheet:	Vishay Semiconductors GmbH (2004)
Temperature	TMP102, Texas Instruments
temperature range:	[-25,85] °C
accuracy within range:	0.5 °C
resolution:	0.0625 °C
tech. datasheet:	Texas Instruments (2007-2008)
Humidity	HIH-5030/5031, Honeywell
total accuracy in [11,89]%RH	± 3 % RH
response time in slow moving air	5 s
operating temperature	[-40,85] °C
tech. datasheet	Honeywell International Inc. (2010)

3.5 Running a typical experiment

In this Section I will describe the typical procedures during an experiment, starting with the germination of the seeds, going through planting of the seedlings to X-raying them. At the end, an overview over the data is provided.

3.5.1 Seed germination

Dry seeds were stored in a dark and dry place. For germination I placed them on a wet paper towel. I then wrapped it in a plastic bag to prevent evaporation of the water and put the plastic bag in a cardboard box to shield the seeds from light. The cardboard box rested on the lab windowsill in the sun for 24 to 48 h. Fig.16 shows a sample of germinated seeds of the same age.

Figure 16: Seedlings after 1,5 days of germination. Seedlings planted into growth cell were ideally 0.5-1 cm long, like the one at the top right. If they are too small, they cannot take up NS, if they are too long, the root breaks during planting.

3.5.2 Planting the seedling

Care is in place when planting the seedlings, because the roots are very sensitive and break when bended. I plant the seedling into the packing by making a 1 cm deep hole with a narrow spoon. I place the seedling onto the inclined spoon and close the hole in the packing around it. Then I start the program controlling the syringe pump and the shell script for reading in the growth conditions. Fig.17 shows the seedling after 2 and 3 days of planting, respectively.

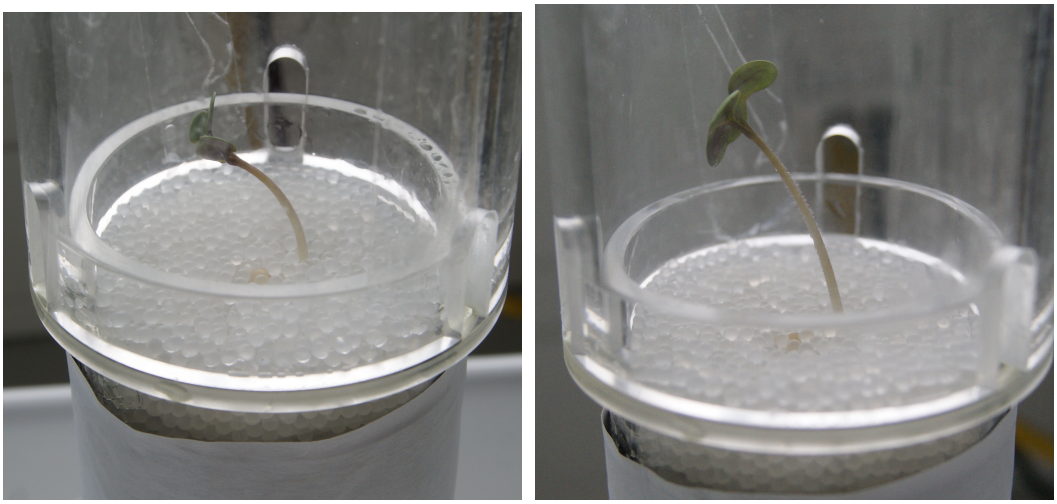

(a) plant 11 on day 2 (b) plant 11 on day 3

Figure 17: Plant growth above ground

3.5.3 X-raying plants

For X-raying the plants I remove the top cylinder of the growth cell, carry the bottom one containing the plant within the packing to the X-ray tomograph and take a scan using the parameters listed in Tab.4. Afterwards I spray water on the plants because of the warm and dry air in the X-ray lab and take the growth cell back to its place. The interval between two X-ray scans is shown for each plant in Fig.18. When the root is longer than the size of one single tomogram, two or three scans have to be taken of the growth cell. Depending on the number of scans this procedure lasts 30 to 90 minutes. The parameters were chosen to exert a minimum amount of stress on the plant while yielding tomograms of serviceable image quality: I keep the beam intensity as low as possible and reduce the total scan time to a minimum, while still capturing data that allow for an accurate detection of the roots and the granular packing. Experience shows that the mustard plants start to wither after 2 hours without NS supply.

Table 4: X-ray parameters used for experiments at hand. Total scan time refers to time needed for one scan. If it was necessary to make two or three scans of the same plant, the time doubles resp. triples.

model:	phoenix nanotom s
manufacturer:	GE Sensing and Inspection Technologies GmbH
acceleration voltage U_{acc}:	80 kV
heating current I_h:	50 μA
number of projections:	900
shots averaged for one projection:	9
shots skipped between projections:	4
exposure time for one shot:	125 ms
total scan time:	24.5 min
detector pixel binning:	4×4
projection size:	556...576 × 572 px = 45.592...49.536 mm
voxel resolution:	0.082...0.086 mm

3.5.4 State of Data

Details of plant growth and lifetimes for various stages in the development of the setup are provided in Fig.18. It also shows at which time instants tomography scans were taken. Tab.5 lists the treatment per plant, e.g. whether or not surfactant was used or which fluid supply method was applied.

Table 5: Plant treatment during growth. Up to plant 9 infusion parameters changed between plants and within the lifetime of single plants. Plant 18 and 19 already died during germination, therefore they are not mentioned here. Horizontal lines are guidance for the eye.

plant #	Fluid supply method †: dripping from above ◯: glass ring $\overline{\wedge}$: nozzle Sec.3.3.2 and 3.3.3	grown in pairs with monitored conditions Sec.3.4 [space]: no monitoring	NS treated with surfactant Sec.3.3.5 ×: yes	NS infusion parameters acc. to Tab.1 on p.31 ×: yes	NS drainage ⊔: dripping into bowl ≀: gravitational drainage ⊗: peristaltic pump Fig.12 on p.31
1	†				⊔
2	†				⊔
3	†				⊔
4	†				⊔
5	◯	a	×	×	⊔
6	◯	a	×	×	⊔
7	◯	b	×	×	⊔
8	◯	b	×	×	⊔
9	$\overline{\wedge}$	c	×	×	≀
10	†	c	×	×	≀
11	$\overline{\wedge}$	d	×	×	≀
12	$\overline{\wedge}$	d	×	×	≀
13	$\overline{\wedge}$	single	×	×	≀
14	$\overline{\wedge}$	e	×	×	⊗
15	$\overline{\wedge}$	e	×	×	⊗
16	$\overline{\wedge}$	f	×	×	⊗
17	$\overline{\wedge}$	f	×	×	⊗

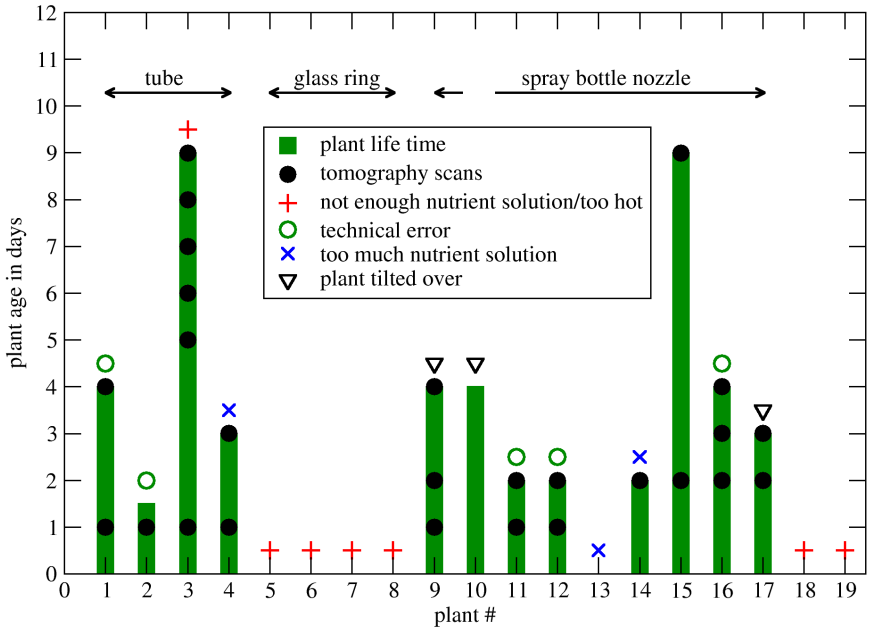

Figure 18: State of Data: Plant life times, CT scanning points, nutrition supply method (horizontal double-ended arrows at the top) and causes for plant deaths (open symbols on top of the green lifetime bars). "Technical error" refers to breakdown of the NS supply system, "Tilt over" means that the the plant was not stable enough to carry its own weight and tilted over. Plants 5-8 and 13 died shortly after planting, 18+19 died during germination. The number of scans usable for analysis is reduced by criteria explained later-on (Sec.5.1)

3.5.5 End of the experiment: cleaning-up

At the end of the experiment, i.e. when the plant has ceased to live or the tap root reaches the bottom of the growth cell, I take out the spheres, removing all root parts, and clean the spheres (for the procedure go to p.79). I disassemble the growth cell and clean it with water and a 50% ethanol solution.[11] I also replace the tubes of the nutrient supply system and clean the syringes with ethanol.

[11]Pure ethanol and acetone lead to dissolution of the glue, Sodium hydroxide corrodes the aluminium parts of the growth cell.

Dried roots vs. green leaves In some cases it is not definitely possible to determine, if the roots had dried or not by looking at the above-ground parts of the plant, as Fig. 19 shows. This makes the definition of the end of plant life-time ambiguous.

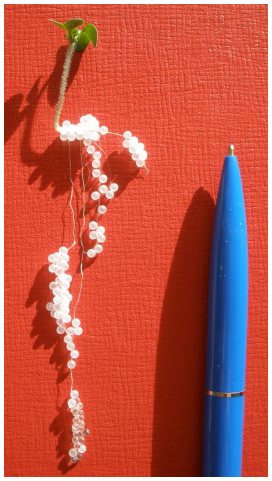

Figure 19: Photo of dried roots on still green plant 3. At several points PP spheres still adhere to the root. (The root sprouts fine hairs during growth that attach to the grains.)

4 Processing 3D CT images

The aim of this Section is to show how the raw image data, i.e. the *tomogram*, from the computer tomograph was processed to yield the exact particle and root coordinates. For this purpose I wrote a set of MATLAB scripts based on code by Song-Chuan Zhao. The process is depicted in the flowchart on page 45:
First, the grey values of the *slices* (the 2D images from the tomogram) were rescaled to remove the inhomogeneity along the radius of the growth cell. For background elimination a first grey threshold was determined using Otsu's algorithm (Otsu, 1979). Then the particle coordinates were retrieved using a combination of defect filling, image erosion, median filtering and a second, manually determined grey threshold (see detailed description below). At the end the root was found half-automatically as one of the largest connected volumes remaining in the tomogram. For the half-automatic part and the visual control of the image processing the imaging tool FIJI (Schindelin *et al.*, 2012) was used. This also goes for the images of tomogram slices in this thesis.

Data format One tomogram consists of an approximately $570 \times 570 \times 570$ matrix of 16 bit unsigned integer (`uint16`) grey values. At a resolution of approximately 80μm per voxel this is a cube of 4.5 cm edge length. The length scales of the tomogram and its relation to the physical growth cell are shown in Fig. 20. The respective file is $\approx$ 400 MB big, so for further processing the data has to be converted to a format that needs less storage space. The grey values of a tomogram do not use the whole `uint16` range of grey values from 0 (black) to 65535 (white) (as can be seen in Fig. 24). Furthermore, the brightest and darkest parts of the tomogram are outside the granular aggregate (see Fig.22). Thus a script by Max Neudecker (`MNCb_Rescale16bit_8bit`) was used to cut off the edges of the histogram. I chose these as maximum and minimum grey values, which belonged to the brightest and darkest spots of the inside of the growth cell. The script then scaled the remaining grey values to the new `uint8` range of $[0, 255]$ to increase the contrast within the aggregate.

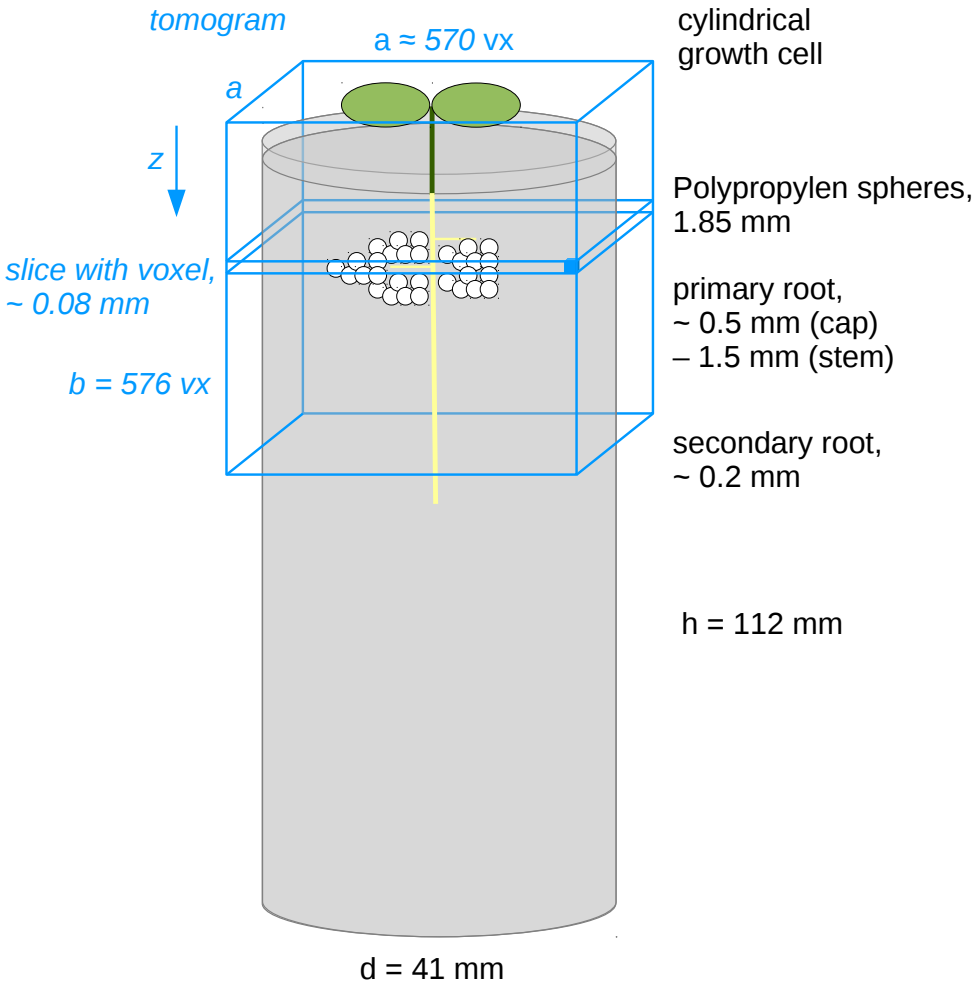

Figure 20: Length scales and relation of cylindrical growth cell (physical) and tomogram (virtual). Numbers refer to diameters/edge lengths. Voxel size, root and particle diameter are not to scale. Slices can also be planes parallel to the z axis but here operations in all but one case were carried out on the slices perpendicular to z. For longer roots two to three tomography scans were taken (see p.58 for details).

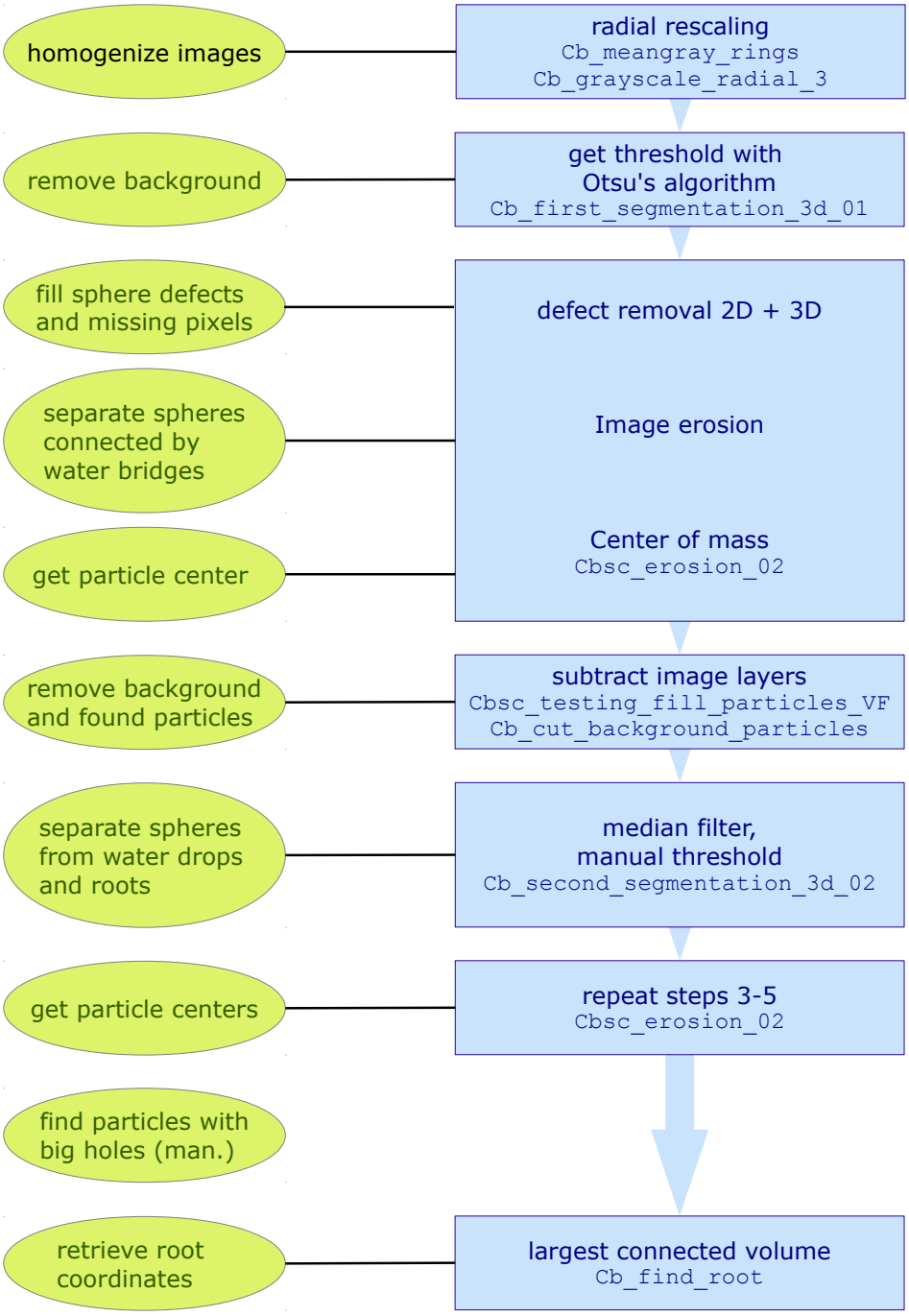

Figure 21: Flowchart for image processing algorithm: The programming steps are shown on the right together with script names in `typewriter style`, their effect on the data is shown on the left.

4.1 Rescaling of tomogram grey values

When looking at the slices of the raw tomogram (Fig.22a) one can see that there is a white ring, which has no physical representation in the growth cell, and that they are generally darker in the middle than at the edges (see Figs.22b and 23). For the global application of a thresholding algorithm this grey value dependency on the radius must be removed or the particles at the border of the cell will be lost.

Creating the rescaling function: To determine the rescaling function, the mean grey value as a function of the slice radius has to be calculated. The slice radius is the distance from any point in the slice to its center. This was done by defining radial bins (*rings*) around the center of the slice and taking the average grey value in each ring. In order to do this the slice information has to be rearranged (see Figure 25):

The slice is represented by a matrix in MATLAB, so one of its entries contains three pieces of information: the grey value g, its row i and column j. The rows and columns are transformed into (x, y) coordinates and the distance of each pixel to the center of the slice is calculated. The pixel information is sorted into a ring. For later access during rescaling this is organized as a $3 \times 50 \times 5200$ matrix or *lookup table*: 3 "layers" contain the original slice indices i, j and the grey values; the 50 "columns" represent the rings with ≈ 5200 entries each. Furthermore, the mean grey value of the whole slice is calculated. In Fig.23b this is plotted versus z. In the beginning, it increases rapidly, stays roughly constant for several hundred slices and then decreases again. The first part corresponds to the air and plant parts (stem and leaves) above the particle aggregate. The second part of the curve represents the bulk of the aggregate. The third part is at the lower edge of the tomogram where the tomogram is generally darker. The average rescaling function is taken of the ca. 400 slices that comprise the bulk to smooth the rescaling function. A *moving average* of the 12 nearest neighbours is applied on the result.

Rescaling The rescaling itself is carried out using the following formula: the grey value is divided by the mean grey value of its respective ring and, to get results in the `uint8` range, multiplied with the average grey value of the whole tomogram. The result is rounded to the next integer:

$$g_{rescaled} = \texttt{uint8}\left(g \cdot \frac{\langle g \rangle_{tomo}}{\langle g \rangle_{ring}}\right) \tag{2}$$

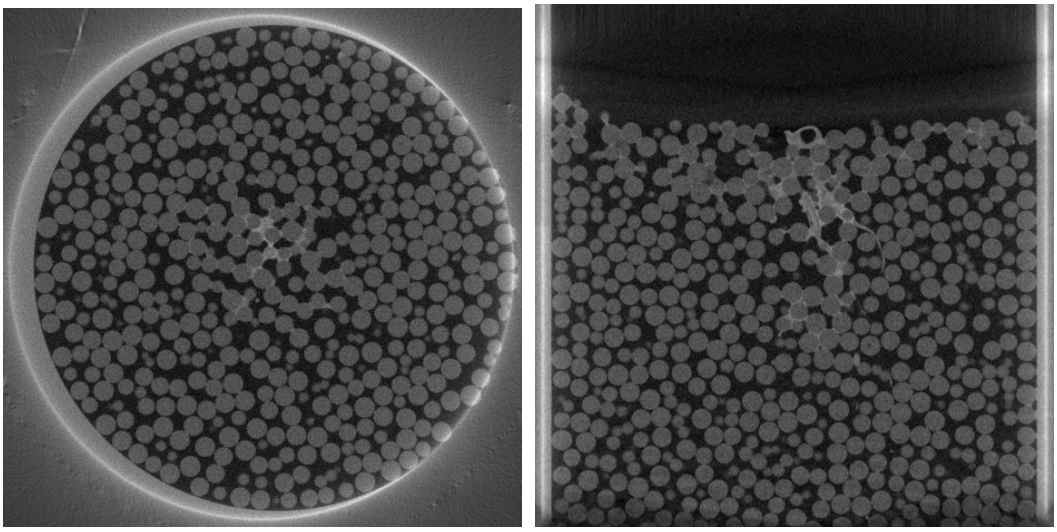

(a) xy plane (b) yz plane

Figure 22: Two slices of the same raw tomogram

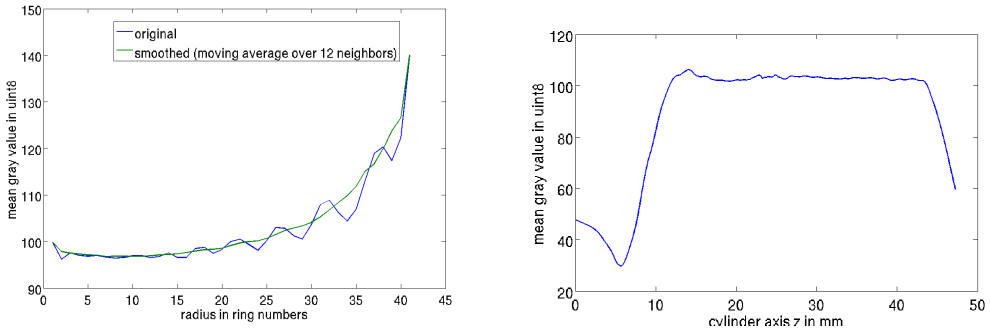

(a) Mean grey value vs. slice radius (b) Mean grey value vs. z axis

Figure 23: Mean grey values of one tomogram, averaged over several slices (23a) or over one slice (23b). The smoothed line in 23a is used as a rescaling function (explained on p.46).

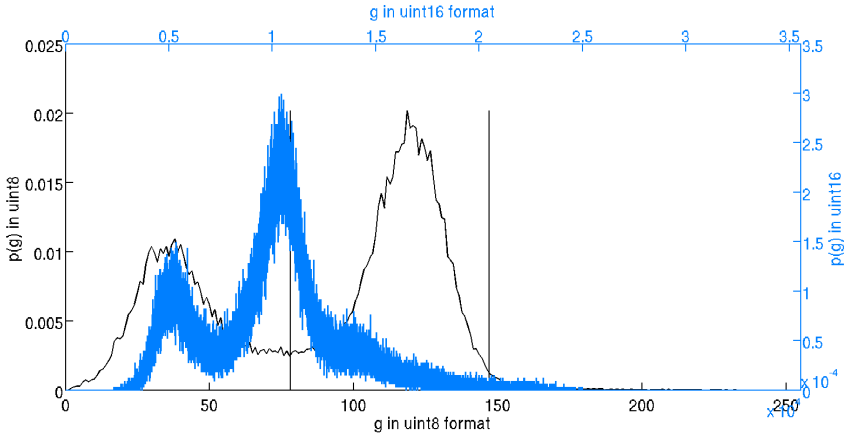

Figure 24: Histograms of raw and rescaled slice with segmentation thresholds (black vertical lines; left: automatic, right: manual threshold). In the `uint8` histogram the area outside of the cell was not taken into account.

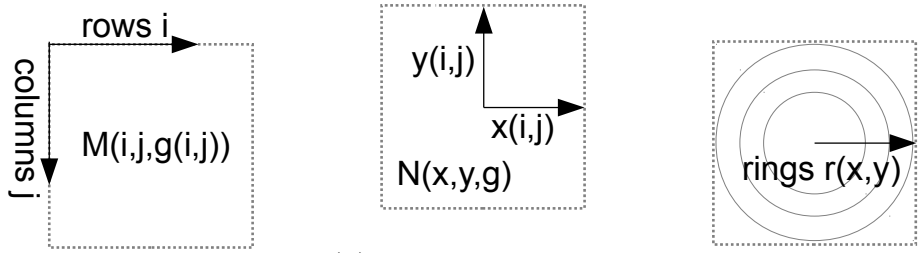

(a) Slice as Matlab matrix M with rows i and columns j, storing grey values g at (i, j)

(b) Slice with centered coordinate system $N(x(i,j), y(i,j), g(i,j))$ as a function of the old rows and columns

(c) Slice as lookup table $T(g(i(r), j(r)))$ with grey values g and their i, j sorted into rings r

Figure 25: Schema showing the transformation (25a to 25b) and sorting (25b to 25c) of slice coordinates into radial bins r while keeping the information on the original coordinates. The dotted square represents the slice in all three sub-figures, g is the grey value.

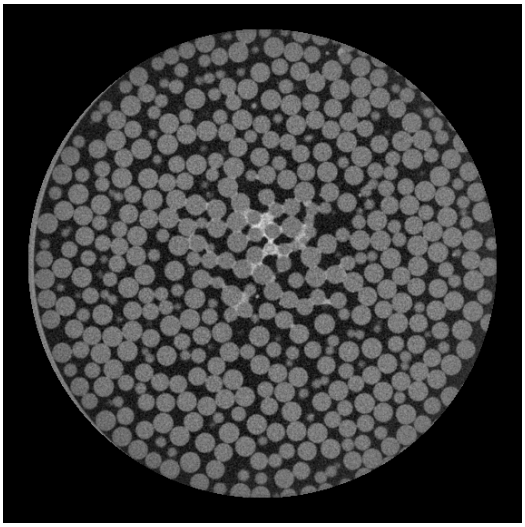

Figure 26: Radially rescaled slice (same slice as in 22a). The area outside the cell was coloured black and not taken into account for faster rescaling and easier threshold computation.

4.2 Tomogram segmentation

The aims of the tomogram segmentation are the determination of the sphere positions in the packing for a future calculation of the packing fraction and the determination of all voxels belonging to the plant's root. The intuitive way to find particles is the following:

1. remove background with first threshold
2. remove water and roots (which are essentially water) with the second threshold
3. separate particles that are still connected by very small spots of water or that are very close to each other by image erosion

The result of this can be seen in Fig.27.

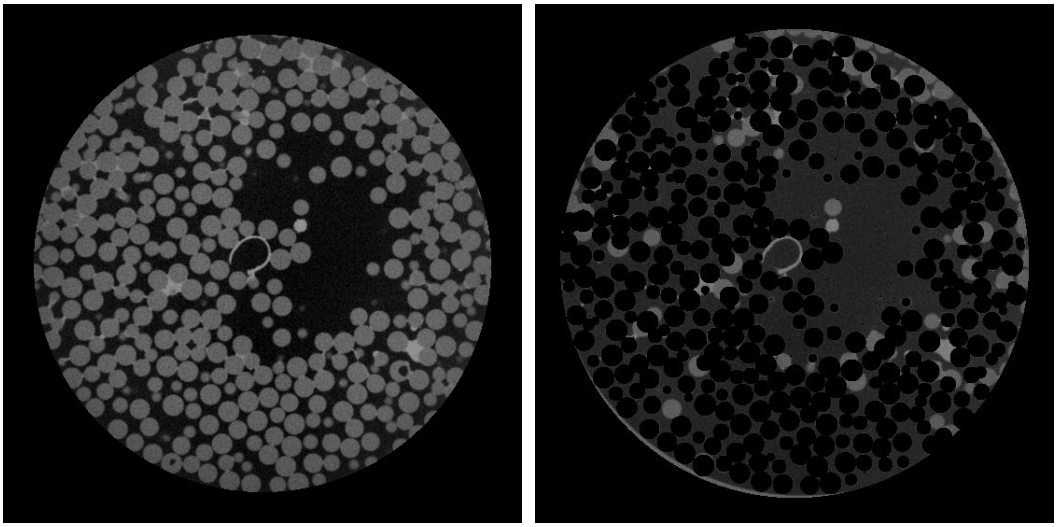

(a) (b)

Figure 27: Result of the simpler two-threshold algorithm: 27a) original (rescaled) slice, 27b) found particles (coloured black)

For the background, this grey threshold-based segmentation is suitable (as will be explained in the following Section 4.2.1), for roots and particles it is not. The difficulty of the image segmentation is the inhomogeneity of the slices: sometimes the space between the particles is filled with water (*water bridge*), sometimes even several particles are surrounded by it (*drops*), sometimes the root is half as thick as the particles, and sometimes it is only a tenth (ca. 2-3 pixels in diameter, see Fig.22b for an example). This results in a very broad

grey value distribution for the roots and the water without a peak in the slice histogram due to the low root diameter and water content. Furthermore, the distribution overlaps with that of the particles (see Fig.24). Therefore, I chose to take an erosion approach instead of a simple segmentation.

4.2.1 Background: Otsu's algorithm

The background, which in this case is represented by the air between particles, roots and water, was removed by using an automatic threshold. This threshold was determined with Otsu's algorithm (Otsu, 1979). This method is based on the histogram of an image: For all grey values in the histogram it divides the histogram into two parts (*classes*) with a threshold t. It then calculates the *within-class variance* which is the sum of the two class variances $\sigma^2_{1,2}$ weighted by the classes' fraction $\omega_{1,2}$ of the total histogram:

$$\sigma^2_w(t) = \omega_1(t)\sigma^2_1(t) + \omega_2(t)\sigma^2_2(t), \tag{3}$$

The t where σ^2_w is minimal is defined as the grey threshold segmenting the image best. A more visual way is to think of it as the point in the histogram where both classes together are as narrow as possible.

As Otsu shows in his paper, it is mathematically equivalent and faster to compute the *between-class variance*:

$$\sigma^2_b(t) = \sigma^2 - \sigma^2_w(t) = \omega_1(t)[\mu_1(t) - \mu]^2 + \omega_2(t)[\mu_2(t) - \mu]^2 \tag{4}$$

($\mu_{1,2}$ being the mean of class 1 or 2 and μ being the mean and σ^2 being the variance of the total histogram) and find that t where σ^2_b has its maximum. One can think of this value as the highest meaningful distance of the two class peaks.

In Fig. 28 this is illustrated by plotting not only the histogram but also the within-class variances and the between-class variances for all possible thresholds. Note that there is a broad interval of serviceable thresholds.

The method works best if the histogram is "well-balanced" and exhibiting two clearly separated regions, meaning the foreground and the background are easy to distinguish in the image, like the slice in Fig. 24. The result is a binarized slice (background black, particles white), see Fig. 29a. Otsu's algorithm can also be adapted to two-, three- or four-level thresholding, but at that point other algorithms are faster (Liao *et al.*, 2001). For an explanation of this algorithm using an example with simple numbers the interested reader is directed to the web page under Greensted (2010).

For the tomograms the threshold was computed individually for each slice. This was necessary because the manner in which the rescaling was

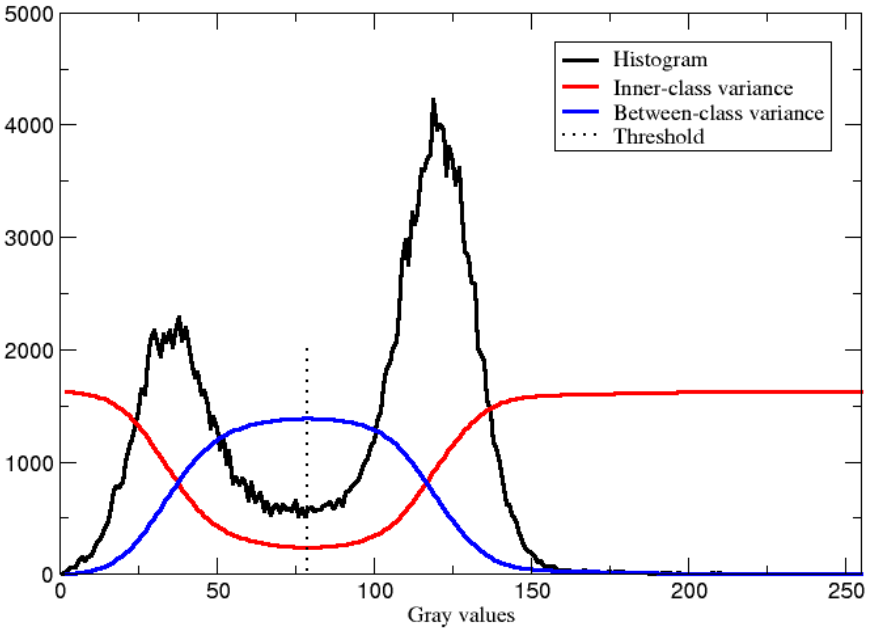

Figure 28: Example histogram with threshold and variances according to Otsu (1979)

done shifted the slice histograms against each other. Using a single threshold from one of the bulk slices on the whole tomogram thus results in individual slices being segmented at the wrong grey level. Also computing a global threshold for the whole tomogram returned wrong binarization especially at the upper and lower end of the tomogram, where the illumination of the slices is different.

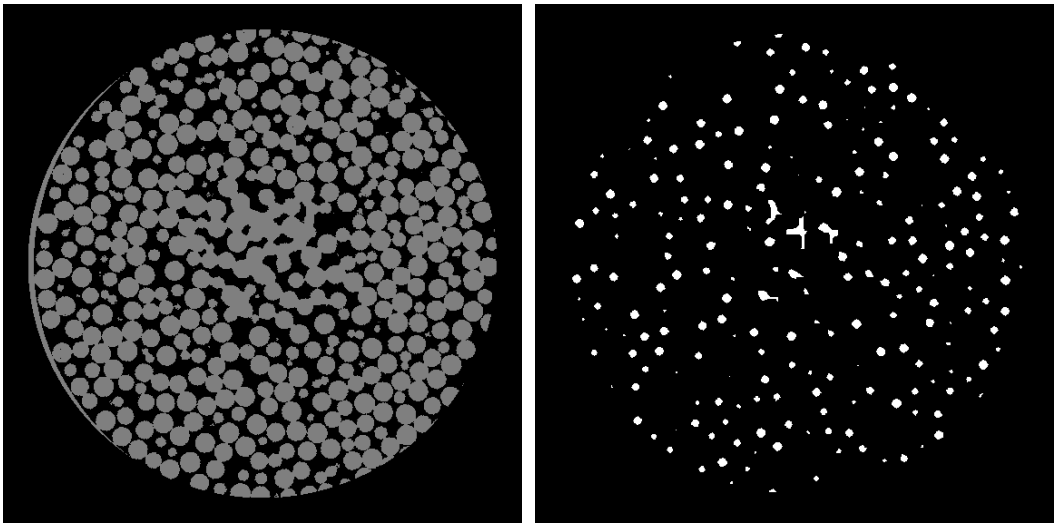

(a) (b)

Figure 29: Binarized (29a) and eroded (29b) slices. The black parts are the background, the white resp. grey parts are particles, water and roots. There appear to be less particles compared to 29a because erosion also removes the particle surface in z direction.

4.2.2 Particles: Image erosion

Erosion and Defects *Erosion* is a technique where the white parts of a binary (black-and-white) image are removed layer by layer. Each pixel of the image is evaluated with respect to its neighbourhood. The evaluated pixel is the center of the erosion matrix. If all pixels in the neighbourhood (or *erosion matrix)* are white, nothing happens. If one of them is black, the evaluated pixel is turned black as well. For the tomograms I used two erosion matrices, a smaller, $3 \times 3 \times 3$ "cubic" one:

$$A_{1kl} == A_{2kl} = A_{3kl} \quad \begin{bmatrix} 1 & 1 & 1 \\ 1 & 1 & 1 \\ 1 & 1 & 1 \end{bmatrix}$$

and a bigger, $5 \times 5 \times 5$ "diamond"-shaped one (only the pixels marked with 1 belong to the environment):

$$B_{1kl} = \begin{bmatrix} 0 & 0 & 0 & 0 & 0 \\ 0 & 0 & 0 & 0 & 0 \\ 0 & 0 & 1 & 0 & 0 \\ 0 & 0 & 0 & 0 & 0 \\ 0 & 0 & 0 & 0 & 0 \end{bmatrix} = B_{5kl}$$

$$B_{2kl} = \begin{bmatrix} 0 & 0 & 0 & 0 & 0 \\ 0 & 1 & 1 & 1 & 0 \\ 0 & 1 & 1 & 1 & 0 \\ 0 & 1 & 1 & 1 & 0 \\ 0 & 0 & 0 & 0 & 0 \end{bmatrix} = B_{4kl}$$

$$B_{3kl} = \begin{bmatrix} 1 & 1 & 1 & 1 & 1 \\ 1 & 1 & 1 & 1 & 1 \\ 1 & 1 & 1 & 1 & 1 \\ 1 & 1 & 1 & 1 & 1 \\ 1 & 1 & 1 & 1 & 1 \end{bmatrix}$$

The bigger the evaluated region per pixel, the stronger the effect of the image erosion. Based on Zhao's code, one erosion cycle with B and three with A were carried out and thus particles connected by water bridges were separated. An example slice is shown in Fig.29b.

To ensure that defects, be they holes in the particles or pixels accidentally removed by the first threshold, do not "destroy" the particles during erosion, they were filled using an algorithm developed by Zhao. It goes through all binarized slices along the z axis of the tomogram, finds connected background areas and sets all areas smaller than a manual threshold to foreground colour. Afterwards the algorithm repeats this procedure with the x and y axes of the tomogram, so that an *open* defect (physically, this corresponds to a hole at the particle surface) in one direction can be filled as a *closed* defect from the other two directions. For an illustration of the technique see Fig. 30, for a more detailed explanation look up p. 68 of his dissertation (Zhao, 2013).

Particle finding I The particles were identified as connected volumes of a certain size range, and their center-of-mass was computed and stored in an external text file. The two size thresholds necessary for this were determined by computing the size distribution of the connected volumes found in the tomogram and taking two values left and right of the greatest, Gaussian-shaped peak. (This was done only once for all tomograms.)

With this procedure ca. 95% percent of the 9000 to 12000 particles were found (see Fig.31). They were coloured black and thus removed from the

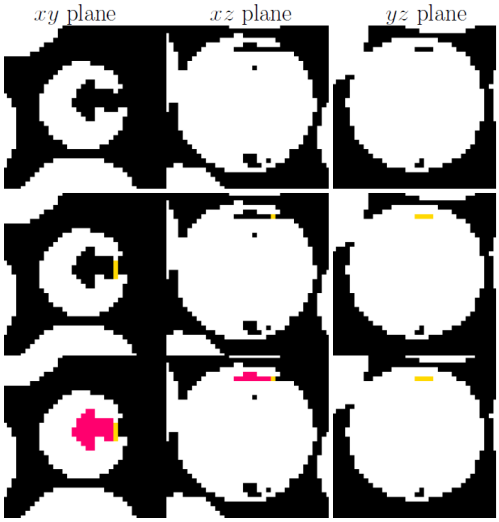

Figure 30: Illustration of the defect filling algorithm. The first row shows the defect along the three axes of the tomogram: it is *open* if looked at from z- and y axis (xy and xz plane resp.) and *closed* from the x axis. In the second row the defect is filled first in the yz plane, which closes it in the other planes, to be completely filled in the third row. (Image taken from Zhao (2013), sphere sizes do not match those used here.)

tomogram using the scripts `testing_fill_beads_VF.m` and `gray_template.m` by Zhao. `insert ref` Those not found were either immersed in drops of water together with other particles, so that they could not be separated by erosion (Figs.29b,31a , or had open defects (Fig.32a). The particle radius in these figures is a rough estimate, precise determination follows in the Results Section (p.65).

Particle finding II To catch also the other particles, the water drops had to be removed as far as possible. For this the background and particles already found were removed from the rescaled slices. Then a *median filter* was applied to reduce the noise and a manual grey threshold was set in a way, that the water drops were at least partly removed while keeping the particles as intact as possible (Fig.31b). (The threshold had to be set manually because of the overlap of the particles' and the root's grey value distribution, see Fig.24), so that the water drops but not the particles were destroyed during erosion. Afterwards the steps (defect removal, erosion, calculating center of mass) of the paragraph above were repeated.

Thus ca. 4% $(350 - 500)$ more particles could be found. The rest $(0.2 - 1.2\% = 20 - 120)$ were either those with large open defects or in a conglomerate

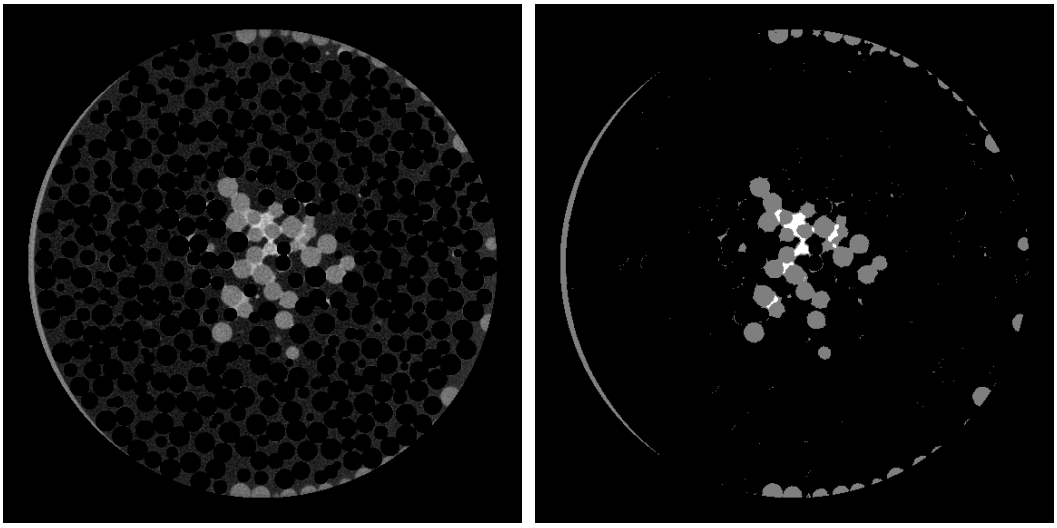

(a) (b)

Figure 31: 31a) Effectiveness of Particle finding I: Particles missed because of their water contact. Found particles are coloured black in the rescaled slice of Fig.26, 31b) Result of slice subtraction: Slice = Fig.29a − 31a + manual second threshold. grey values above the threshold are set to white.

within a water drop. Their coordinates had to be determined by hand (see Fig.32).

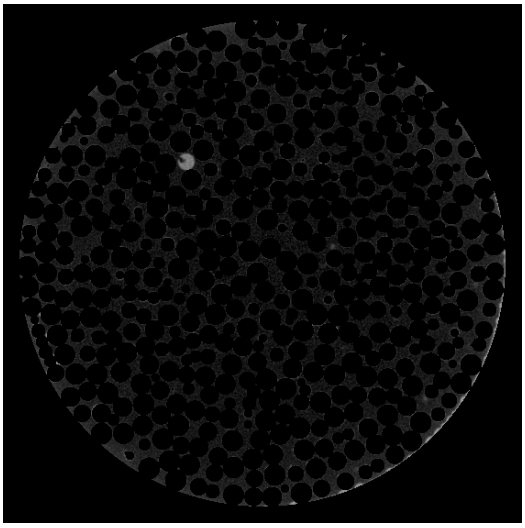

(a) Particle missed because of a hole that is at its surface.

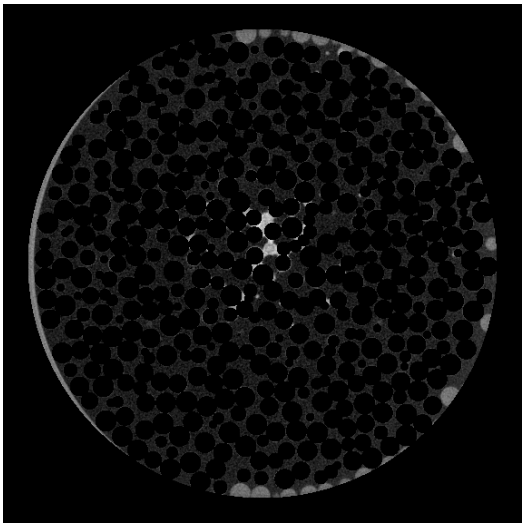

(b) Effectiveness of second particle finding.

Figure 32: Result of Particle finding II. Found particles coloured black in rescaled slice Fig. 26

4.2.3 roots

To finally retrieve the pixels belonging to roots from the tomogram, these steps were applied:

1. elementwise multiplication of binary tomogram matrix of removed background (Fig. 29a) with that of removed particles (Fig. 32) and with rescaled tomogram (Fig. 26) → creates tomogram containing only roots + water
2. identify connected 3D regions → root/root touching water; water drops; parts of growth cell margin
3. remove objects too large or too small with manual threshold
4. inspect cleared tomogram with imaging tool (e.g. Fiji), find appropriate thresholds for step (3) by iteration
5. save list of root coordinates to text file

The root is often but not always the largest connected volume in the tomogram. If the water content in the growth cell at the time of the tomography scan was very high, the largest volumes in the tomogram are water drops or the root in contact with one or more water drops. In that case the root

coordinates could not be completely isolated from the water because of their similar grey values.

4.3 3D images of the root

At the end the root was visualized using the 3D image rendering program POVRAY (see Fig. 33). Povray uses a list of objects, the position and direction of a virtual camera, and the position and direction of one or more light sources to create a three-dimensional image[12]. In this case the list of objects was the list of root coordinates as 1 voxel-sized cubes.

4.4 If the root is longer than the tomogram

For tomograms consisting of multiple overlapping scans (Fig. 20 shows that one tomography volume compares to a third of the growth cell) the root coordinates from different scans were transformed to the same coordinate system by using the height difference in pixel. Double root voxel entries were removed from the list. As the particle finding gave positions in a subpixel resolution, this method could not be used for the particles, so for the determination of the sphere diameter the scans were treated as separate tomograms.

[12]The principle is similar to that of the typesetting system LaTeX, just for images

Figure 33: 3D image of the root of plant 3 at the 9th day of growth. The non-cylindrical objects attached to the root are water droplets that could not be separated from the root. Image created using POVRAY

5 Results

In this section I will first describe, which of the data produced during the development of the setup I will analyse. I then show how the size of the root can be determined quantitatively and finally determine the diameter of the spheres in the granular packing, which is necessary for the future calculation of the packing fraction.

5.1 Data chosen for analysis

In order to measure the size of the root as a function of time I chose to analyze subsequent tomograms with respect to these criteria:

- mechanically undisturbed packing and plant between scans
- root free of water drops (image processing could not separate the root from the drop, see Section 4 for details)
- root not touching the wall (same separation problem)

The tomograms that fulfilled the criteria were 2 and 3 of plant 9 (see p.41 for a plot showing the amount of scans per plant); 1 and 2 of plant 11; 1 and 2 of plant 15; and 2 and 3 of plant 16. Of these, plant 15 had to be left out because the particle finding algorithm found only 80-90% of 10,000 resp. 12,000 spheres due to a very high water content in the growth cell.

5.2 Root volume vs. time

In order to determine the size of the root as a function of its age, two definitions have to be set: the zero point for the time axis, i.e. the "moment of birth" of the plant and the point where the stem turns into the root.

5.2.1 Plant age definition

For the zero point there are three candidates:

1. the moment where the seeds are put onto a wet paper towel for germination
2. the moment where the radicle breaks the shell of the seed
3. the moment where the germinated seed is planted into the granular aggregate

I chose the third option for the following reason: Germination takes 24 h to 48 h, depending on many factors. The biological diversity among plants of the same species both plays an important role while being out of experimental control at the same time. Thus the first point looses its meaning as a precise zero point. It would also have required an inconsiderable technical effort to catch the precise moment of germination. Fig.16 shows that even seeds germinating under the same conditions have different growth rates and/or germination points. Hence, I chose the moment where the germinated seed had a length of 0.5-1 cm to be plant age $t = 0$. At this point no tomography scan could be done, otherwise the root would dry out while it is not connected to the water supply. Therefore, I estimated the volume V_0 of the root as a cylinder (length 7 mm and diameter 1 mm) of 5 mm^3 (using the photo of the germinated seeds in Fig.16.

5.2.2 Root size and error

In Fig.34 the volume change of the root on two subsequent days is plotted for three plants. The growth rate ranges from approximately 5 to 25 mm^3 per day. The computation of an average is meaningless with only three data points of this range.

In order to probe the reaction of the granular aggregate to the growth of the root, I consider the root as that part of the stem, which grows below the surface of the aggregate. I estimated the surface roughness of the packing to be one particle layer (at sphere diameter d =1.85 mm) and I determined the cross-sectional areas of the three roots at this depth from the tomogram slices in order to get an estimated error of the root volume:

$$\begin{aligned} \Delta V_{root} &= \mathrm{surface} \quad \mathrm{roughness} \times \mathrm{cross-sectional} \quad \mathrm{root} \quad \mathrm{area} \\ &= 2 \ldots 5\,\mathrm{mm}^3 \end{aligned} \tag{5}$$

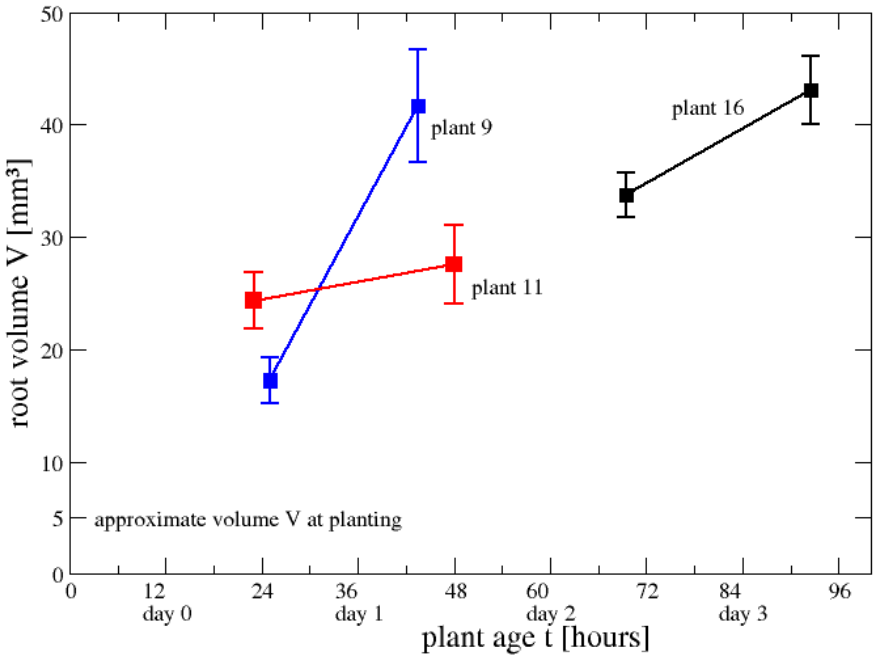

Figure 34: Change of root volume during the period of one day. Data taken from 3 different plants under different conditions (see Fig.35). Plant age $t = 0$ denotes the moment of planting. y error bars computed with equation (5)

5.2.3 Growth conditions

For the two plants that were scanned at similar points in their growth and that have the highest difference in their growth behaviour, the growth conditions (temperature, relative humidity and illuminance) are plotted in Fig.35.[13]

Notable characteristics of the conditions are:

- high temperature changes during morning until early afternoon for both plants (up to 8 °C)
- high fluctuations of the relative humidity (up to 30% rel. humidity), with humidities below 40% before noon (plant 11) or around noon (plant 9) resp.

[13]The curve of plant 16 was omitted because the maximum illuminance of the light sensor was exceeded during the day.

- similar temperatures during the night (about 23 °C) between 6 pm and 6 am)
- fluctuating illuminance, with times of illuminance > 400 lux coinciding to times of temperature peaks
- temperature and light have different values during night and day, and they also differ in their fluctuation behaviour from night and day
- humidity has no reproducible day-night-behaviour

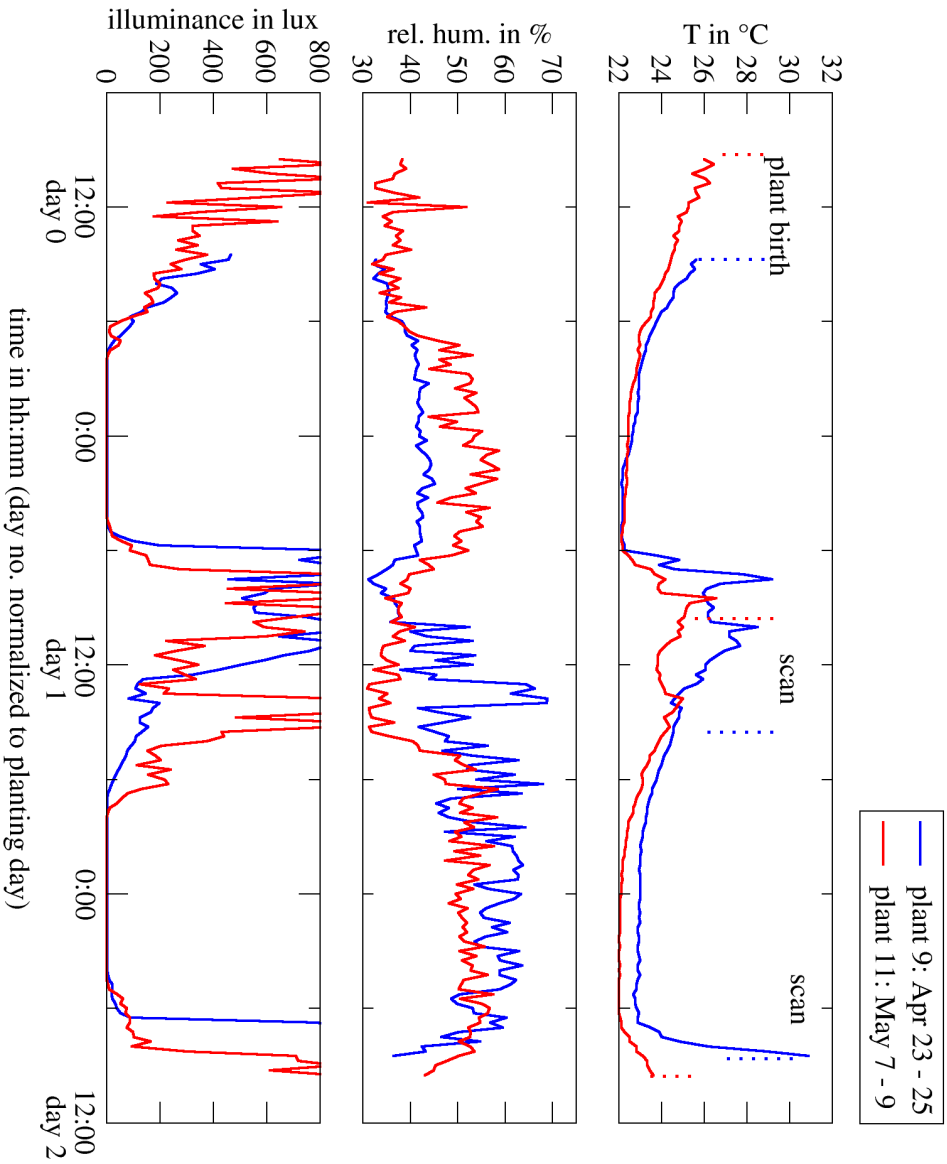

Figure 35: Growth conditions for two plants (same colour coding as in Fig.34). Time axes are aligned with day-night cycle; moments of planting and scanning are denoted by vertical dotted lines for consistency with Fig.34; measurement were taken every 15 min.

5.2.4 Discussion

Comparing the actual growth of the roots in Fig.34 with the external conditions plotted in Fig.35 does not yield a simple correlation. The behaviour of the monitored parameters is too complex while the data (conditions and growth rate) is too sparse for a statistical analysis. Furthermore, there is another parameter that I could not monitor even though it has a direct impact on root growth, namely the water content of the soil, or the granular packing, respectively (p.29).

I cannot correlate the seasonal temperature behaviour with the growth conditions, but from Fig.35 I can derive that the sunlight coming in from South-East has a direct influence on the light and temperature development in the growth cell. The interaction between temperature and relative humidity is not trivial and I cannot enlighten is further with the data in 35.

In order to develop the experiment further, I make the following suggestions:

1. increasing the number of simultaneously grown plants for a statistical analysis

2. greenhouse: placing the growth cells into a container of size $\sim 1\,m \times 1\,m \times 1\,m$ in order to control humidity and temperature; note that gas exchange must be allowed due to carbon dioxide and oxygen use and production

3. as a consequence of the first bullet point: upscale the nutrient supply with a set of micro valves that can be programmed to open sequentially, keeping the pressure in the tubes at the necessary level without requiring more syringe pumps

5.3 Characterization of the spheres

As this study was motivated by the aim to quantify the local environment of the root and its influence on the root growth, the sphere diameter needs to be determined, so that as a later step the global and local packing can be calculated. The sphere diameter d was determined by calculating the pair-correlation function (PCF) with the script `Raps` by Weis (2013-2015) of the bulk particles and fitting a Gaussian distribution to the first peak. The bulk consists of all particles that are no closer than 2 particle diameters (as given by the manufacturer) to the wall (see Fig.36). I chose this definition to avoid the crystallization effect of the packing close to the wall. The presence of the root in the packing might falsify the result, so as a comparison the

PCF of two packings without roots inside were computed. An example PCF is shown in Fig.37.

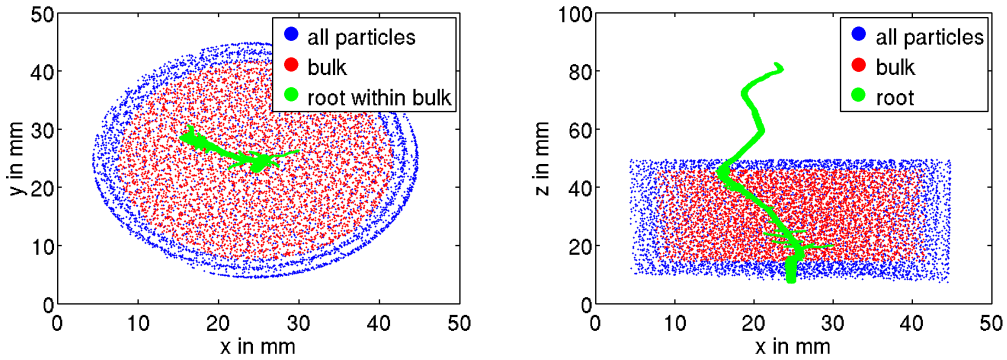

Figure 36: BULK DEFINITION: Projections of particle positions and root voxels onto xy-and xz-plane. Note that tip of the root is at positive z values (i.e. the root is "pointing upwards")

The pair-correlation function is not a Gaussian distribution, neither is the first peak – note its asymmetry in Fig.37: the values of $g(x)$ below 1.84 are converging to zero, whereas the values above 1.9 are at approximately 200. The shape of the first peak and its width are determined by two factors: the diameter distribution of the spheres and the quality of the position determination by the image processing algorithm. It would be necessary to take a sample of known diameter distribution to validate the algorithm and to thus quantify their influence on the peak shape. I have neither a reference sample nor a validated code, therefore, I make these assumptions:

1. I assume, that the manufacturing process has no bias towards smaller or bigger particles.

2. I also assume, that the algorithm has neither a bias towards any axis of the tomogram for the determination of the sphere position nor that I had such a bias during the manual position determination of the spheres the algorithm did not find.

Therefore, I use a Gaussian distribution to fit the first peak of the PCF.

I added a scaling factor a to account for non-normalization, and an offset b to account for the vertical shift of the data points (as compared to a Gaussian distribution):

$$f(x) = \frac{a}{\sqrt{2\pi}\cdot\sigma}\exp\left(\frac{-(x-d)^2}{2\cdot\sigma^2}\right) + b \tag{6}$$

(σ is the standard deviation of the distribution.)

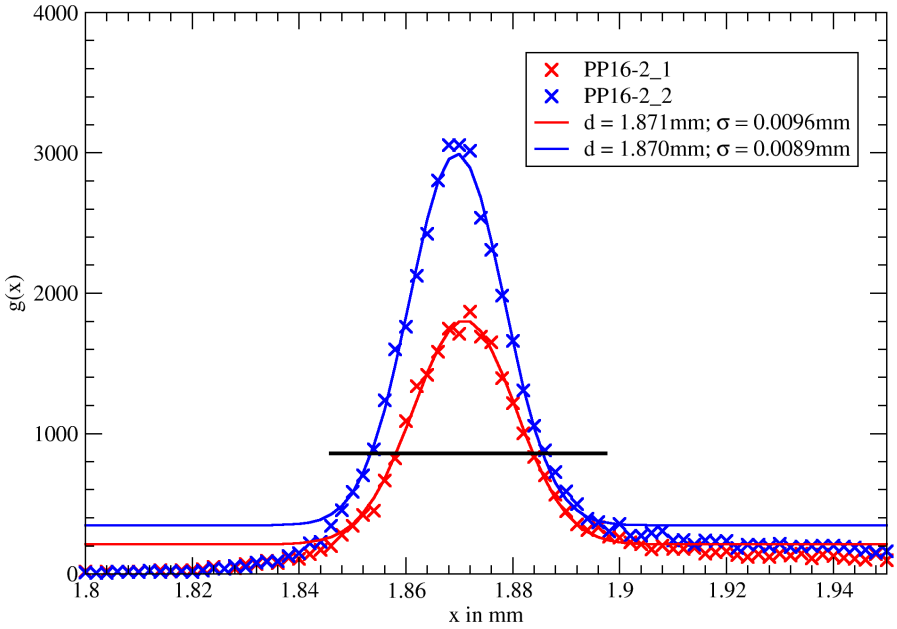

Figure 37: First peak of pair-correlation function for upper and lower part of tomogram 16-2. The fit was obtained using eq.(6) and carried out on the interval denoted with the black horizontal line.

I defined the fitting range to be in the interval [1.84,1.9], given the shape of the PC and the expected value of the particle diameter (1.85 mm according to the manufacturer SPHEROTECH).

The resulting diameters can be found in Table 6. The mean sphere diameter, as determined with the Gaussian fit of the PCF, is 1.870 μm with a statistical error of 0.001 μm. The peak is on average 0.01 μm wide (average σ from the fit), which is smaller than the deviation range given by the manufacturer. This suggests that the spheres have a better monodispersity than the manufacturer assures and that also the sphere detection algorithm is precise enough to preserve this result. (If the fit curves were wider than the manufacturers tolerance, this could still imply a high sphere monodispersity but then the code with a would cause the scatter around the mean.) Also the sphere diameter determined from the packings without root lies still in the range of the statistical error.

Table 6: Diameters determined using the Pair-correlation function compared to manufacturer's data. σ is the standard deviation from the fit

plant-scan#	d in mm	σ in mm
9-2	1.870	0.0093
9-3	1.871	0.0097
11-1	1.870	0.0089
11-2_1	1.870	0.0094
11-2_2	1.869	0.0095
16-2_1	1.871	0.0096
16-2_2	1.870	0.0089
16-3_1	1.871	0.0100
16-3_2	1.872	0.0102
16-3_3	1.871	0.0111
without root:		
9-4	1.870	0.0087
17-1_2	1.870	0.0089
mean of all $d \| \sigma$	1.870	0.0095
standard dev. of the mean	0.001	
SPHEROTECH	1.85	0.03

5.4 Summary

Plants of white mustard were grown in an aggregate of polymethylene spheres, using an automated nutrient solution supply system driven by a syringe and a peristaltic pump for the nutrient solution. At a daily rate, X-ray tomograms were taken of the root within the aggregate. After subtracting background, particles and water from the tomograms, the size of the root could be determined for 3 plants. The growth rate varies between 5 and 25 mm^3 per day. The growth conditions were being monitored, but showed no correlation to the growth rate. The mean diameter of the spheres necessary for the calculation of a local and global packing fraction was determined as $1.87\,\mathrm{mm} \pm 0.001\,\mathrm{mm}$ using the pair-correlation function from the bulk of the sphere packings.

6 Conclusion

Motivated by the question how a plant root interacts mechanically with the soil I set out to investigate root growth with X-ray computed tomography. In contrast to other studies I did not grow the plant (Sinapis alba L., white mustard) in soil but, taking a physicists approach, I model soil as a granular medium of mono-disperse spheres. The advised choice of this model soil, the plant species and observation methods allow me to study the impact of root growth on the soil and vice versa with unprecedented detail. The progress of the study are presented in the three parts of the present diploma thesis:

Setup: I devised a setup (and documented its development) that enables me to grow two mustard plants simultaneously in sphere packings. The setup consists of two cylindrical growth cells with a continuous, closed-cycle water and nutrient supply. The fluid supply is driven by a syringe pump (infusion) and a peristaltic pump (removal). Sensors monitoring illuminance, temperature and humidity within the cells are read out by a SHELL script. During setup development I grew 17 mustard plants and repeatedly scanned the roots with an X-ray computer tomograph. In order to obtain high-quality images of roots, it was important that the setup admits drainage so that tomograms are taken of (nearly) dry sphere packings.

3D Image processing: I wrote a MATLAB routine segmenting the image phases (roots, rest water, spheres, air) and retrieving positions of root voxel and sphere centres. After homogenization, the air phase is segmented using Otsu's algorithm. Roots, spheres and rest water are segmented by a combination of image erosion, a manual gray threshold and image subtraction. Positions of spheres are found as centers of (voxel) mass of connected regions, the root is found as one of the largest connected region. For automatic image processing a high quality of the algorithm is of central importance. My routine misses less than 0.35% of the spheres in a tomogram.

Experimental results: I show that the positions of the root voxel can be used to quantitatively determine root structure parameters: I calculate the volume of selected plants on subsequent days at a precision of 10 to 20%, finding a growth rate between 5 and 25 mm^3 per day. I also determine the sphere diameter with a pair-correlation function and find its error to be smaller than the mono-dispersity given by the manufacturer. This suggests that the image processing algorithm is precise enough to preserve this mono-dispersity.

7 Outlook

The next step of the analysis will be the calculation of the local packing fraction with a Voronoi tesselation before and after the root tip has entered a certain region. This contributes an answer to the question, whether the tip avoids denser regions above a threshold packing fraction.

As next steps in the experimental part I would build a climate chamber with controlled humidity and temperature and up-scale the fluid supply to get more replicates. Furthermore, in order to determine the effect of the radiation on the root/plant growth, the following control experiments can be conducted:

1. Grow a set of plants and repeatedly scan them with the computer tomograph.

2. Grow a second set of plants under the same conditions, take them to the X-ray CT lab, but *do not scan them*. Thus this set of plants receives the same environmental stress without the radiation – the X-ray CT lab is dark, warmer and more arid than the optimal growth conditions, furthermore the plants are without fluid supply for a certain amount of time.

3. Grow a third set of plants under the same conditions as 1 and 2, but do not scan them nor take them to the X-ray CT lab.

At the end also scan the two control groups compare root structure parameters such as root volume, diameter and length with that of the first set of plants.

In a further step may be also interesting to explore root growth for a plant with thicker roots, thus considering a different ratio of root and sphere diameter.

The decision to use a dry sphere packing as a growth medium instead of soil allowed me to follow root growth with non-destructive high-quality 3D imaging. However, as a personal remark I would like to add, that it is *much* more difficult to grow a plant in plastic spheres than at home in a pot. If there is an interest to continue these or similar experiments, I therefore suggest that two people work on this topic: one focusing on setup building, the other on programming and data analysis.

References

Bengough, Anthony G. & Mullins, Chris E. 1990 Mechanical impedance to root growth: a review of experimental techniques and root growth responses. *Journal of Soil Science* **41** (3), 341–358. URL: http://onlinelibrary.wiley.com/doi/10.1111/j.1365-2389.1990.tb00070.x/abstract.

Beste, Andrea 2015 Industrielle Landwirtschaft mit Zukunftsproblemen. In *Bodenatlas – Daten und Fakten über Acker, Land und Erde* (ed. Annette Maennel). Heinrich-Böll-Stiftung, Berlin.

Brandt, Wilhelm, Gürke, M., Köhler, F. E., Pabst, G., Schellenberg, G. & Vogtherr, Max. 1883 *Köhler's Medizinal-Pflanzen in naturgetreuen Abbildungen mit kurz erläuterndem Texte*. Gera-Untermhaus: Fr. Eugen Köhler. URL: http://www.biodiversitylibrary.org/bibliography/623 [cited 19 December 2014].

Chamovitz, Daniel 2012 *What a plant knows – A field guide to the senses of your garden*, 1st edn. Oxford, UK: Oneworld Publications.

Chen, Guihua, Weil, Ray R. & Hill, Robert L. 2014 Effects of compaction and cover crops on soil least limiting water range and air permeability. *Soil and Tillage Research* **136**, 61–69. URL: http://www.sciencedirect.com/science/article/pii/S0167198713001621.

Clapham, Arthur R., Tutin, Thomas G. & Warburg, Edmund F. 1962 *Flora of the British isles*, 2nd edn. Cambridge: University Press.

Cvrčková, Fatima, Lipavská, Helena & Žárský, Viktor 2009 Plant intelligence. *Plant Signaling & Behavior* **4** (5), 394–399. URL: http://dx.doi.org/10.4161/psb.4.5.8276.

Ehlers, Knut 2015 Das unsichtbare Ökosystem. In *Bodenatlas – Daten und Fakten über Acker, Land und Erde* (ed. Annette Maennel). Heinrich-Böll-Stiftung, Berlin.

Epstein, Emanuel & Bloom, Arnold J. 2004 *Mineral Nutrition of Plants: Principles and Perspectives*, 2nd edn. Sunderland, Mass: Sinauer Associates.

Fargašová, A. 1999 Determination of metal interactions on root growth of sinapis alba seedlings. *Biologia Plantarum* **42** (4), 637–640. URL: http://link.springer.com/article/10.1023/A%3A1002608324204.

Gagliano, Monica, Mancuso, Stefano & Robert, Daniel 2012 Towards understanding plant bioacoustics. *Trends in Plant Science* **17** (6), 323–325. URL: http://www.sciencedirect.com/science/article/pii/S1360138512000544.

Greensted, Andrew 2010 The lab book pages: Otsu thresholding. URL: http://www.labbookpages.co.uk/software/imgProc/otsuThreshold.html [cited 8 January 2015].

Hargreaves, Caroline E., Gregory, Peter J. & Bengough, Anthony Glyn 2008 Measuring root traits in barley (hordeum vulgare ssp. vulgare and ssp. spontaneum) seedlings using gel chambers, soil sacs and x-ray microtomography. *Plant and Soil* **316** (1-2), 285–297. URL: http://link.springer.com/article/10.1007/s11104-008-9780-4.

Heeraman, Deo A., Hopmans, Jan W. & Clausnitzer, V. 1997 Three dimensional imaging of plant roots in situ with x-ray computed tomography. *Plant and Soil* **189** (2), 167–179. URL: http://link.springer.com/article/10.1023/B%3APLSO.0000009694.64377.6f.

Hillnhütter, C., Sikora, R. A., Oerke, E. C. & van Dusschoten, D. 2012 Nuclear magnetic resonance: a tool for imaging belowground damage caused by heterodera schachtii and rhizoctonia solani on sugar beet. *Journal of Experimental Botany* **63** (1), 319–327. URL: http://jxb.oxfordjournals.org/lookup/doi/10.1093/jxb/err273.

Hoagland, Dennis R & Arnon, Daniel I 1938 The water-culture method for growing plants without soil. Circular 347. University of California, Agricultural Experiment Station, Berkeley.

Honeywell International Inc. 2010 Humidity sensor HIH-5030 technical datasheet. URL: http://www.tinkerforge.com/de/doc/Hardware/Bricklets/Humidity.html [cited 18 December 2014].

Jaeger, Heinrich, Nagel, Sidney & Behringer, Robert 1996 Granular solids, liquids, and gases. *Reviews of Modern Physics* **68**, 1259–1273. URL: http://jfi.uchicago.edu/~jaeger/group/JaegerGroupPapers/granular/Granular_RMP.pdf.

Johnson, Edna L. 1936 Susceptibility of seventy species of flowering plants to x-radiation. *Plant Physiology* **11** (2), 319–342. URL: http://www.ncbi.nlm.nih.gov/pmc/articles/PMC439213/.

Kolb, Evelyne, Hartmann, Christian & Genet, Patricia 2012 Radial force development during root growth measured by photoelasticity. *Plant and Soil* **360** (1-2), 19–35. URL: http://link.springer.com/10.1007/s11104-012-1316-2.

Liao, Ping-sung, Chen, Tse-sheng & Chung, Pau-choo 2001 A fast algorithm for multilevel thresholding. *Journal of Information Science and Engineering* **17**, 713–727.

Lohmann, Maité, Scheu, Stefan & Müller, Caroline 2009 Decomposers and root feeders interactively affect plant defence in sinapis alba. *Oecologia* **160** (2), 289–298. URL: http://www.ncbi.nlm.nih.gov/pmc/articles/PMC3085730/.

Lynch, Jonathan P. & Wojciechowski, Tobias 2015 Opportunities and challenges in the subsoil: pathways to deeper rooted crops. *Journal of Experimental Botany* p. eru508. URL: http://jxb.oxfordjournals.org/content/early/2015/01/11/jxb.eru508.

Mayer, Johannes G., Uehleke, Bernhard & Saum, Pater Kilian 2002 *Handbuch der Klosterheilkunde*. München: Zabert Sandmann.

Meier, Ina C., Pritchard, Seth G., Brzostek, Edward R., McCormack, M. Luke & Phillips, Richard P. 2015 The rhizosphere and hyphosphere differ in their impacts on carbon and nitrogen cycling in forests exposed to elevated CO2. *New Phytologist* **205** (3), 1164–1174. URL: http://onlinelibrary.wiley.com/doi/10.1111/nph.13122/abstract.

Mooney, S. J., Pridmore, T. P., Helliwell, J. & Bennett, M. J. 2011 Developing x-ray computed tomography to non-invasively image 3-d root systems architecture in soil. *Plant and Soil* **352** (1-2), 1–22. URL: http://link.springer.com/10.1007/s11104-011-1039-9.

Moradi, Ahmad B., Carminati, Andrea, Vetterlein, Doris, Vontobel, Peter, Lehmann, Eberhard, Weller, Ulrich, Hopmans, Jan W., Vogel, Hans-Jörg & Oswald, Sascha E. 2011 Three-dimensional visualization and quantification of water content in the rhizosphere. *New Phytologist* **192** (3), 653–663. URL: http://doi.wiley.com/10.1111/j.1469-8137.2011.03826.x.

Murison, Julie Lynette 2014 Wetting heterogeneities in porous media. PhD thesis, Georg-August-University, G\"{o}ttingen. URL: https://ediss.uni-goettingen.de/handle/11858/00-1735-0000-0022-5E9C-2.

Neumann, Günter, George, Timothy S. & Plassard, Claude 2009 Strategies and methods for studying the rhizosphere—the plant science toolbox. *Plant and Soil* **321** (1-2), 431–456. URL: http://link.springer.com/article/10.1007/s11104-009-9953-9.

Otsu, Nobuyuki 1979 A threshold selection method from gray-level histograms. *IEEE Transactions on Systems, Man, and Cybernetics* **9** (1), 62–66. URL: http://ieeexplore.ieee.org/lpdocs/epic03/wrapper.htm?arnumber=4310076.

Platten, David 1998 Understanding imaging performance (3): Artefacts. URL: http://www.impactscan.org/slides/impactcourse/artefacts/.

Poorter, Hendrik, Bühler, Jonas, van Dusschoten, Dagmar, Climent, José & Postma, Johannes A. 2012 Pot size matters: a meta-analysis of the effects of rooting volume on plant growth. *Functional Plant Biology* **39** (11), 839. URL: http://www.publish.csiro.au/?paper=FP12049.

Schindelin, Johannes, Arganda-Carreras, Ignacio, Frise, Erwin, Kaynig, Verena, Longair, Mark, Pietzsch, Tobias, Preibisch, Stephan, Rueden, Curtis, Saalfeld, Stephan, Schmid, Benjamin, Tinevez, Jean-Yves, White, Daniel J., Hartenstein, Volker, Eliceiri, Kevin, Tomancak, Pavel & Cardona, Albert 2012 Fiji: an open-source platform for biological-image analysis. *Nature Methods* **9** (7), 676–682. URL: http://www.nature.com/nmeth/journal/v9/n7/full/nmeth.2019.html.

Schröter, Matthias, Nägle, Sibylle, Radin, Charles & Swinney, Harry L 2007 Phase transition in a static granular system. *Europhysics Letters* **78** (4), 44004. URL: http://stacks.iop.org/0295-5075/78/i=4/a=44004?key=crossref.87675ec9768adfeef50e961490ace8eb.

Silverberg, Jesse L., Noar, Roslyn D., Packer, Michael S., Harrison, Maria J., Henley, Christopher L., Cohen, Itai & Gerbode, Sharon J. 2012 3d imaging and mechanical modeling of helical buckling in medicago truncatula plant roots. *Proceedings of the National Academy of Sciences* **109** (42), 16794–16799. URL: http://www.pnas.org/cgi/doi/10.1073/pnas.1209287109.

Smith, Steven W. 1997 *The Scientist and Engineer's Guide to Digital Signal Processing*, 1st edn. California Technical Publishing.

Strasburger, Eduard, Bresinsky, Andreas, Körner, Christian, Kadereit, Joachim W., Neuhaus, Gunther & Sonnewald, Uwe 2008 *Lehrbuch der Botanik*, 36th edn. Heidelberg: Spektrum, Akad. Verl.

Tabtabaei, Solmaz & Diosady, Levente L. 2013 Aqueous and enzymatic extraction processes for the production of food-grade proteins and industrial oil from dehulled yellow mustard flour. *Food Research International* **52** (2), 547–556. URL: `http://www.sciencedirect.com/science/article/pii/S0963996913001683`.

Texas Instruments 2007-2008 Temperature sensor TEMT6000 technical datasheet. URL: `http://www.tinkerforge.com/de/doc/Hardware/Bricklets/Temperature.html` [cited 18 December 2014].

Vishay Semiconductors GmbH 2004 Ambient light sensor. URL: `http://www.tinkerforge.com/de/doc/Hardware/Bricklets/Ambient\_Light.html\\` [cited 18 December 2014].

Wantanabe, K., Mandang, T., S., Tojo, Ai, F. & Huang, B.K. 1992 Non-destructive root-zone analysis with x-ray ct scanner. American Society of Agricultural Engineers, St. Joseph, MI, USA, paper No. 92-3081, not online available.

Weis, Simon 2013-2015 RAPS: Random and packed structure investigation. URL: `https://bitbucket.org/Laguna_999/raps` [cited 9 January 2015].

Wendell, D.M., Luginbuhl, K., Guerrero, J. & Hosoi, A.E. 2011 Experimental investigation of plant root growth through granular substrates. *Experimental Mechanics* **52** (7), 945–949. URL: `http://www.springerlink.com/index/10.1007/s11340-011-9569-x`.

Withington, Jennifer M., Elkin, Adrienne D., Bułaj, Bartosz, Olesiński, Jakub, Tracy, Keena N., Bouma, Tjeerd J., Oleksyn, Jacek, Anderson, Laurel J., Modrzyński, Jerzy, Reich, Peter B. & Eissenstat, David M. 2003 The impact of material used for minirhizotron tubes for root research. *New Phytologist* **160** (3), 533–544. URL: `http://doi.wiley.com/10.1046/j.1469-8137.2003.00903.x`.

Zappala, Susan, Helliwell, Jonathan R., Tracy, Saoirse R., Mairhofer, Stefan, Sturrock, Craig J., Pridmore, Tony, Bennett, Malcolm & Mooney, Sacha J. 2013 Effects of x-ray dose on rhizosphere studies using x-ray computed tomography. *PLoS ONE* **8** (6), e67250. URL: `http://dx.doi.org/10.1371/journal.pone.0067250`.

Zhao, Song-Chuan 2013 Length scales in granular matter. PhD thesis, Georg-August-University, Goettingen, (matlab scripts not published). URL: https://ediss.uni-goettingen.de/handle/11858/00-1735-0000-0015-9D98-C.

Zou, C., Sands, R., Buchan, G. & Hudson, I. 2000 Least limiting water range: a potential indicator of physical quality of forest soils. *Australian Journal of Soil Research* **38** (5), 947. URL: http://www.publish.csiro.au/?paper=SR99108.

A Setup supplements

A.1 Technical drawing of the growth cell

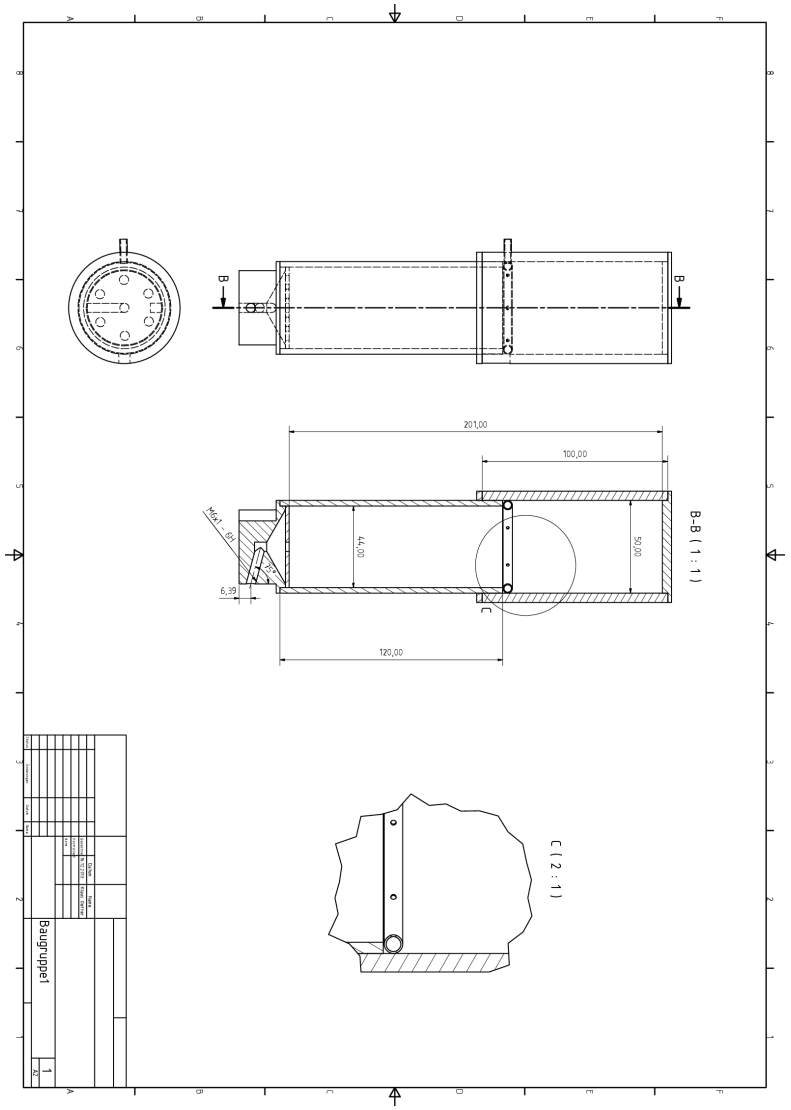

Figure 38: Technical drawing of growth cell (done by mechanics workshop of Bayreuth University). The glass ring is the same as in Fig.14.

A.2 script for reading out environment conditions from Tinkerforge bricks

Execution of shell script `environment.reader.sh` yields a file `plant-environment.txt`, which contains the temperature, humidity and ambient light read in every 15 minutes from the TINKERFORGE bricklets. This is the command for execution (termination with CTRL + C):

```
watch -n 900 -t -p ./environment.reader.sh
```

This is the script:

```
./read_temp >> plant-environment.txt
./read_hum >> plant-environment.txt
./read_light >> plant-environment.txt
date +"%F%_R" >> plant-environment.txt
```

The programs `read_temp`,`read_hum`,`read_light` are C code available on the TINKERFORGE website and can be compiled using the following line

```
#gcc -pthread -o read_temp read_temp.c ip_connection.c
bricklet_temperature.c
```

A.3 Recipe for nutrient solution

Table 7: Recipe for Real modified Hoagland's solution (Hoagland & Arnon (1938), Epstein & Bloom (2004))

	concentration [g/l]	volume [ml]
Macronutrient		
KNO_3	101.1	6
$Ca(NO_3)_2$	236.16	4
$NH_4 \cdot H_2PO_4$	115.08	2
$MgSO_4$	246.49	1
Micronutrient		all together: 1
KCl	3.728	
H_3BO_3	1.546	
$MnSO_4 \cdot H_2O$	0.338	
$ZnSO_4 \cdot 7\,H_2O$	0.575	
$CuSO_4 \cdot 5\,H_2O$	0.124	
H_2MoO_4 (85% MoO_3)	0.080	
Iron		
Fe-EDTA	6.922	1

A.4 Cleaning particles

Chemicals	concentration
NaOH solution	250 mMol/l = 10 g/l
desionized water	
isopropanol:water	1:2
Utensils	
scale	
high vessel	
magnetic stir bar	
sieve	

Procedure

1. spheres with magnetic stir bar in NaOH for 30 min (removes organic rests)
2. clean spheres 3 times in sieves with desionized water
3. spheres with magnetic stir bar in isopropanol (removes fats)
4. clean spheres 3 times in sieves with desionized water
5. dry in oven at 50 °C in flat vessel (10-12 hours)

B Glossary

This glossary contains biology, physics and computer science jargon I used in this thesis (without the intention of being comprehensive). Some of the words, especially botanic terms, in the glossary are not present in the thesis, nevertheless, I found them helpful while reading the literature cited in the references. All words are listed with their English and, if available, German jargon. Sometimes also an abbreviation is provided if it seemed to me omnipresent.

8 bit unsigned integer (uint8)
: data format: one pixel or matrix entry can have the size of 8 bit (refers to the precision of the entry), meaning a numeric range of 0 to 255 ($255 = 2^8 - 1$)

angiosperm Bedecktsamer
: group of plants that flower

annual plant Einjährige
: the full life cycle of the plant takes place within one year

apoplastic apoplastisch
: transport within the cell wall (parallel to it)

Arabidopsis thaliana (common wall-cress) Ackerschmalwand
: most important plant for botanical molecular genetics because of its very short (sequenced) genom and life cycle

attenuation Abschwächung
: in physics: weakening of a beam, e.g. an X-ray beam on its way through matter

ballotini Ballotini, Glaskügelchen
: poly- or mono-disperse glass spheres around 1mm, used e.g. in pressurized cells for estimating root penetration resistance, or for cleaning metal surfaces

binary image Schwarzweiß-Bild
: image where all pixels are either black or white

Brassicaceae, also: mustards Kreuzblütengewächse
: plants whose 4 petals look like a cross

central cylinder Zentralzylinder
: inner part of the root responsible for upward water transport and stability of the root

computed tomography scan (CT scan) Computertomographieaufnahme
the act that produces the tomogram. Sometimes more than one scan is needed to create a tomogram of the full object

dicotyledon Zweikeimblättrige
plant with two seed leaves

erosion (of an image) Bilderosion
method to separate loosely connected image regions of similar gray value by removing their outer edge pixel-wise

fan beam tomograph Fächerstrahltomograph
computer tomograph that creates very thin horizontal slice at different heights that have to be combined for a 3D tomogram

fine earth Feinerde
soil with grain size lower than 2 mm (German classification of grain sizes)

gravitropism Gravitropismus
biological ability to follow gravitational force

histogram Histogramm
diagram plotting all occurring values of a data set against their frequency of occurrence (here used mostly in an image processing context)

horizon Horizont
biological term for "soil layer", they are classified regarding particle size, nutrient content and water retainability

humus Humus
see topsoil

Hydro-culture (Hydrokultur, aquaponisch (biol.))
average plant owner: plant grown in clay granules; plant biologist: plant grown completely in water (also "hydroponics")

hypocotyl Hypocotyl
part of stem of germinating plant between root and seed leaf

laser sheet scanning Laserstrahlabtastung
a method to visualize the behaviour of a 2-component system, where one component is an a laser-excitable fluid: the laser beam is shaped like a plane that moves through the sample, exciting the atoms of one component of the system. When the atoms return to their normal state, they send out photons collected with a camera. These can be reconstructed to yield a 3D representation of the excitable (fluid) component resp. its negative, the unexcitable (e.g. solid) component

lateral/horizontal root Nebenwurzel/Seitenwurzel
root growing sideways, they are responsible for water and nutrient uptake

least limiting water range (llwr) Indicator for soil quality: it defines a range in soil water content within which plant growth is least likely to be limited by the availability of water and air in soil and the soil strength (Zou *et al.*, 2000)

loblolly pine Weihrauchkiefer
a sort of pine native to the southeastern US

lookup table (lut) Nachschlagetabelle
storing data (i.e. parameters, calculation results, material constants, words) in a table so that it dösn't have to be recalculated/measured

magnetic resonance tomography (MRT, NMRI, MRI) also: nuclear magnetic resonance imaging, or: magnetic resonance imaging
deutsch Magnetresonanztomographie, ugs. Kernspintomographi);
3D imaging method based on the magnetic behaviour of the atomic nuclei; mostly used for imaging of soft, i.e. tissues containing water or lipids

mechanical impedance mechanischer Widerstand
Also: root penetration resistance or soil strength: the mechanical resistance of the soil against root growth ($Q = F_{\text{normal}}/A_{\text{rootcrossection}}$)

median filter Medianfilter
Pixels are replaced by the median gray value of their environment → reduces noise, but also contrast (image processing)

median Median
value in a data set that splits the set into equal parts above and below this value (less sensitive to extreme data than the mean)

mono-disperse monodispers
a sample of spheres that have the same diameter (within a small tolerance of 5%)

moving average (with window size n) gleitender Durchschnitt
smoothing a line of data points by replacing each point with the average of its n neighbors. The more neighbors one includes in the average, the smoother the line

mykorrhiza Mykorrhize
class of fungi that lives in symbiosis with the roots of most plant species. They help the plant with the uptake of water and nutrients, but the mechanism behind it and other aspects of the root-fungus relationship is still a field of intense biological research.

nematodes Nematoden, Fadenwürmer
: small white worms living in wet soil, often parasitic to roots, some of them dangerous to humans

non-return valve Rückschlagventil
: valve that allows water flow only in one direction (fluid mech.)

Otsu's algorithm Histogram-based method to determine a threshold (image processing)

packing fraction Packungsdichte
: same as volume fraction

photoelastic photoelastisch
: same as stress-birefringent

phototropism Phototropismus
: biological ability to follow light signals

poly-disperse polydispers
: opposite of mono-disperse: sphere diameters have a wide diameter distribution (different from bi-disperse, i.e. a sample with two occurring, distinct sphere diameters)

pore space Porenvolumen
: the space in soil that consists of air-filled holes ("pores")

porosity Porosität
: density or distribution of pores in porous medium like soil or foam

primary root Haupt-/Primärwurzel
: first order root/main root in a plant root system (develops from radicle)

radicle Keimwurzel
: first root a plant develops already inside the seed, becomes primary root

rhizobia Knöllchenbakterien
: strain of bacteria in symbiosis with roots

rhizosphere Rhizosphäre
: direct soil environment of the roots

rhizotron apparatus for studying roots: box with one or more transparent sidewalls, in which the plant is growing in soil

root elongation Wurzelverlängerung
: the root growing in length

root hairs Wurzelhaare
very fine ($< 100\mu$m) hairs growing from the sides of tap root and lateral root

root nodules Wurzelknöllchen
nutrient storage chamber attached to the root, developed in symbiosis with rhizobia

root window apparatus for studying roots: glass or plexiglas plane inserted vertically into the ground next to plant with some additional space for root observation

rooted plants Landpflanzen
plants living on solid ground

secondary root Sekundärwurzel
root growing from primary root, often synonym to lateral root while specifying the point in root hierarchy

seed leaves Keimblätter
leaves formed during germination (already inside the seed)

shoot Spross
upmost growing part(s) of the stem

slice Scheibe, Schnittbild
one 2D image from the tomogram, usually perpendicular to the rotational axis of the cell

soil strength Bodenwiderstand
see mechanical impedance

stem Sprossachse
above earth part of plant growind upwards (without leaves)

stress-birefringent doppelbrechend unter Belastung
some materials change the refraction index of light depending on the mechanical load they experience. Using an optical filter (circular polarizers) one can see which region in the object is subject to how much mechanical stress.

subsoil Unterboden, Anreicherungsschicht
soil layer below topsoil consisting of sand, silt and clay particles, very low content of organic matter

symplastic symplastisch
transport through the cytoplasm

tap root Pfahlwurzel
root that grows straight downward in search of water (in contrast to spread root)

target part of a x-ray tube in which the X-rays are produced by impacting electrons

tee T-Stück
piece to connect 3 pipes (fluid mech.)

tomogram Tomogramm
the three-dimensional image produced by a computer tomograph

topsoil Oberboden, Humus
upmost soil layer consisting of dead organic matter that has been processed by the microorganisms living in it

volume averaging if a voxel contains a bit of root and a bit of soil, the attenuation value will be the average of both root and soil, i.e. somewhere between their true attenuation values

volume fraction Packungsdichte
the amount of volume of objects filling a container divided by the container volume

voxel Voxel
smallest volume unit in a tomogram, a 3D pixel